The PRC2.1 Subcomplex Opposes G1 Progression through Regulation of CCND1 and CCND2

Adam D. Longhurst[1,2], Kyle Wang[3,4], Harsha Garadi Suresh[3], Mythili Ketavarapu[5,6], Henry N. Ward[7], Ian R. Jones[8,9], Vivek Narayan[8], Frances V. Hundley[1,2,10] Arshia Zernab Hassan[11], Charles Boone[3,4], Chad L. Myers[7,10], Yin Shen[8,12,13], Vijay Ramani[5,6], Brenda J. Andrews[4], David P. Toczyski[1,6,13]

[1]University of California, San Francisco, San Francisco, CA 94158, USA
[2]Tetrad Graduate Program, University of California, San Francisco, San Francisco, CA 94158, USA
[3]Department of Molecular Genetics, University of Toronto, 160 College Street, Toronto, Ontario M5S 3E1, Canada
[4]The Donnelly Centre for Cellular and Biomolecular Research, University of Toronto, Toronto, ON, Canada
[5]Gladstone Institute for Data Science and Biotechnology, J. David Gladstone Institutes, San Francisco, CA, USA
[6]Department of Biochemistry and Biophysics, University of California San Francisco, San Francisco, CA, USA
[7]Bioinformatics and Computational Biology Graduate Program, University of Minnesota – Twin Cities Minneapolis MN USA
[8]Institute for Human Genetics, University of California, San Francisco, San Francisco, CA, USA
[9]Pharmaceutical Sciences and Pharmacogenomics Graduate Program, University of California
[10]Department of Cell Biology, Blavatnik Institute of Harvard Medical School, Boston, MA 02115, USA
[11]Department of Computer Science and Engineering, University of Minnesota – Twin Cities Minneapolis MN USA
[12]Department of Neurology, University of California, San Francisco, San Francisco, CA, USA
[13]Weill Institute for Neurosciences, University of California, San Francisco, San Francisco, CA, USA
[14]Lead Contact

[*]Correspondence: david.toczyski@ucsf.edu (D.P.T.)

Abstract

Progression through the G1 phase of the cell cycle is the most highly regulated step in cellular division. We employed a chemogenomics approach to discover novel cellular networks that regulate cell cycle progression. This approach uncovered functional clusters of genes that altered sensitivity of cells to inhibitors of the G1/S transition. Mutation of components of the Polycomb Repressor Complex 2 rescued growth inhibition caused by the CDK4/6 inhibitor palbociclib, but not to inhibitors of S phase or mitosis. In addition to its core catalytic subunits, mutation of the PRC2.1 accessory protein MTF2, but not the PRC2.2 protein JARID2, rendered cells resistant to palbociclib treatment. We found that PRC2.1 (MTF2), but not PRC2.2 (JARID2), was critical for promoting H3K27me3 deposition at CpG islands genome-wide and in promoters. This included the CpG islands in the promoter of the CDK4/6 cyclins CCND1 and CCND2, and loss of MTF2 lead to upregulation of both CCND1 and CCND2. Our results demonstrate a role for PRC2.1, but not PRC2.2, in promoting G1 progression.

Introduction

Cellular decisions to grow and divide are made by assessing the balance of activating and inhibitory inputs that govern the transition between cell cycle phases. Regulated progression through the cell cycle is crucial for normal cellular growth and organismal development[1–3]. Progression from G1 into S phase is the most highly regulated step of the cell cycle, as initiating DNA replication commits a cell to divide and is frequently mutationally activated in tumors. Cyclin Dependent Kinase 4 (CDK4) and the related CDK6 (henceforth referred to collectively as CDK4/6) play critical roles in promoting G1 progression through phosphorylation of the retinoblastoma protein (RB1). Phosphorylation relieves RB1-mediated transcriptional repression of E2F transcription factors, which are then competent to drive transcription of genes necessary for progression into S phase[3–6]. Because of their crucial role in regulating G1 progression, specific inhibitors targeting CDK4/6 have proven to be effective therapeutics. Palbociclib was the first FDA approved CDK4/6 inhibitor and highly efficacious in the treatment of HR+/HER2- breast cancers, followed by the structurally related molecules ribociclib and abemaciclib[7–11]. However, this classical model of G1 regulation has recently given way to a more complex model[12–14], underscored by the complexity of genetic alterations that lead to resistance to treatment with CDK4/6 inhibitors[4,12,13,15]. Thus, while G1 progression has been the focus of intense study, our understanding of its regulation remains incomplete.

The Polycomb Repressive Complex 2 (PRC2) was initially identified in Drosophila as a developmental regulator that represses the expression of Hox genes[16]. The PRC2 complex is conserved in throughout eukaryotes[17–21] and catalyzes the mono-, di- and tri-methylation of Histone 3 Lysine 27 (referred to collectively as H3K27me3, the fully methylated form of H3K27) and thereby acts as a transcriptional repressor[20]. The core PRC2 complex is composed of a H3K27me3 "reader" EED, a scaffold protein SUZ12, and the catalytic subunit EZH2 (or the more poorly-expressed and less catalytically active paralog EZH1[22]). This core complex is capable of catalyzing H3K27me3 deposition and chromatin association, but how PRC2 achieves full spatiotemporal regulation of chromatin localization and catalytic activity has been an area of active investigation. Recent studies have identified additional accessory factors that modify the localization and enzymatic activity of these core components[23]. The associated auxiliary factors define different PRC2 subcomplexes, which are called PRC2.1 and PRC2.2, based on the composition of the subunits associated with the core PRC2 complex (reviewed in[24,25]). In addition to the core PRC2 subunits, PRC2 .1 consists of two modules, one module containing a Polycomb-like (PCL) protein PHF1, MTF2 or PHF19 and a second module of either PALI1/2 or EPOP. The more homogenous PRC2.2 always consists of the core PRC2 subunits in complex with both JARID2 and AEBP2. The role of these complexes in different cellular processes and contexts is debated. Despite the lack of an a clear analogous sequence to the Polycomb Response Elements which promotes PRC2 chromatin association in *Drosophila*[26,27], the presence of a DNA-binding extended

homology domain in each PCL protein has been proposed to recruit PRC2.1 to unmethylated CpG islands and establish H3K27me3[28,29]. In contrast, PRC2.2 localizes to sites utilizing pre-existing mono-ubiquitinated H2AK119 (H2AK119ub1), which is deposited by the PRC1 complex[30–33], through a ubiquitin interaction motif contained within JARID2[31,32,34,35]. Regardless of their specific roles in the propagation of H3K27me3 histone marks, members of both PRC2.1 and PRC2.2 have been implicated as both positive and negative regulators of stem cell maintenance, differentiation and cancer, depending on the cellular context[25,36–42]. All of the PRC2 core subunits (EZH2, SUZ12 and EED) have been shown to inhibit that transcription of both positive and negative regulators of G1/S progression, including the CDK4/6 protein inhibitor p16[43–47]. However, the net result of these opposing effects on cell cycle progression, and the contribution of the individual subcomplexes to this regulation, rained unclear.

To identify novel regulators of cellular proliferation, we utilized a whole-genome chemogenetic approach to identify genes that sensitized or lent resistance to inhibitors of different cell cycle stages. We uncovered novel resistance mechanisms to three known inhibitors of cell cycle progression in the human haploid cell line HAP1. This approach revealed that mutations in mitochondrial function or the Polycomb complexes rescued slow growth in palbociclib. We could recapitulate these positive genetic interactions pharmacologically using small molecule inhibitors of either PRC2 activity or mitochondrial respiration. Loss of core PRC2 members or PCL subunits of the PRC2.1 subcomplex, particularly MTF2, resulted in resistance to palbociclib, while loss of PRC2.2-specific subunits resulted in sensitivity. Data from CUT&RUN and RNA sequencing experiments performed on clonal MTF2Δ and JARID2Δ knockout mutant cell lines suggest that PRC2.1 plays a more critical role in repressing gene expression when compared with PRC2.2 in HAP1 cells, particularly at promoters containing CpG islands. D-type cyclins are among the genes that are repressed by PRC2.1 and loss of MTF2 results in increased expression of both CCND1 and CCND2 through loss of H3K27me3 in their promoters. This increased expression resulted in an apparent increase in CDK4/6 kinase activity and S-phase entry of cells, driving resistance to CDK4/6 inhibition. Our results suggest that PRC2.1 plays a strong role in G1 progression.

Results

Chemogenetic CRISPR-Cas9 Screen Utilizing Cell Cycle Inhibitors Identified Novel Players in the Cell Cycle

Recently, CRISPR-Cas9 knockout genetic screens have emerged as a powerful way in which to probe genetic interactions[48–50], with the haploid human cell line HAP1serving a popular model for these studies[51–56]. To identify novel genes involved in cell cycle regulation, we carried out genome-wide CRISPR-Cas9 chemogenomic screens in HAP1 cells treated with each of three well-characterized inhibitors of cell cycle progression: palbociclib (a CDK4/6 and G1 progression inhibitor), colchicine (a microtubule polymerization and mitosis inhibitor) and camptothecin (a Topoisomerase I and S/G2 inhibitor). We used a concentration for each inhibitor that reduced cellular proliferation by 30-50% (Fig S1A) (see also [51]) and confirmed their effects on cell cycle progression (Fig. S1B). We then performed a CRISPR-Cas9 whole-genome screen for each of the three inhibitors (Fig. 1A) by introducing the Toronto Knockout Library[57] via lentiviral transduction into a HAP1 cell line constitutively expressing Cas9. Following puromycin selection for two days, cells were propagated in either DMSO (Mock) or in the presence of drug (Treated) for eighteen days. Following propagation, genomic DNA was extracted from the initial and final pools and subjected to deep sequencing, and gene-compound interactions were determined using the Orobas pipeline (source code - Supplemental File 1, chemogenomics screen results -Table S1 and S2). A gene was considered as being significantly enriched or de-enriched in a given condition if both the Loess-adjusted differential gene effect between mean Treated and Mock control was ±0.5 and the FDR<0.4.

This approach resulted in the recovery of predicted compound-gene interactions demonstrating the robustness of both the screen and our analysis approach. For example, targeting of genes known to play roles in DNA Damage Repair (DDR)[58,59], including RAD54L, MUS81 and sixteen proteins in the Fanconi Anemia pathway, strongly sensitized cells to camptothecin, which generates protein-DNA adducts (Fig. 1B and 1C). The molecular target of camptothecin, TOP1[60], is the most resistant gene in the camptothecin screen, as are proteins involved in p53 transcriptional regulation, such as TP53BP1 and STAGA members TAF2, TAF4, TAF5, TAF11 and TAF13 (Fig. 1B). Similarly, colchicine sensitized cells to the mutation of genes encoding proteins involved in mitotic spindle assembly, nuclear division and cytoskeletal assembly, such as CLASP1, DLGAP5 and KNTC1 (Fig. 1D and 1E). Interestingly, inactivation of genes involved in the adaptive immune system, such as BIRC6, UBA5 and USP14, also resulted in sensitivity to colchicine. This observation is intriguing, as colchicine is used clinically as an immunomodulator in the treatment of gout[61]. CCNE1, CDK6, CDK2, CCND2 and CCND1, all of which are integral to promoting the G1/S phase transition, ranked as the 2nd, 24th, 27th, 29th and 46th most important genes for palbociclib resistance, respectively (Fig. 1F and 1G). CCND1 and CCND2 bind either CDK4 or CDK6, the molecular targets of palbociclib, whereas CDK2 and CCNE1 form a related CDK kinase that promotes the G1/S transition. Similarly, cells with sgRNAs targeting RB1, whose phosphorylation by CDK4/6 is a critical step in G1 progression, displayed substantial resistance to palbociclib. The recovery of genes known to function in the relevant biological processes supports the strength of this dataset and bolstered our confidence to use the results obtained to identify novel chemical-genetic interactions.

Chemogenomics Screen Uncovered Novel Genetic Interactions Involved in Response to Inhibitors of Cell Cycle Progression

To identify genes whose inactivation rendered cells sensitive or resistant to a specific cell cycle perturbation, we compared how the Orobas-calculated differential gene effect for a given targeted gene varied in each compound across our CRISPR-Cas9 screen. The majority of genes that conferred either sensitivity or resistance were specific to only one cell cycle inhibitor, with little overlap between the multiple conditions, suggesting that we identified genes that play roles in distinct biological processes (Fig. 2A and Fig S1C). For example, genes encoding DNA repair proteins, mitotic spindle components, and CDK2/4/6 holoenzyme components were only required for proliferation in camptothecin, colchicine, and palbociclib, respectively. We found that only thirteen and twenty genes resulted in sensitivity or resistance, respectively, in every conditions tested and were deemed non-specific and excluded from any further analysis (see Table S2).

We next turned our attention to unexpected and novel compound-gene interactions. To probe these interactions, we analyzed genes that significantly altered response to our three compounds using the gene annotation and analysis portal Metascape and the protein-protein interaction network analysis STRING. In addition to DDR genes, Metascape and STRING analysis of the results of our camptothecin treatment revealed de-enrichment for sgRNAs targeting genes encoding members of the KICSTOR complex (KPTN, SZT2, ITFG2 and KICS2), which negatively regulates mTOR. In contrast, sgRNAs targeting of genes involved in RNA metabolism and chromatin organization increased resistance to this drug (Fig. 2B-2D). It has been suggested that mTOR is involved in attenuating the DDR response through phosphorylation of RNF168, leading to its degradation[62], which could provide one explanation of the observed sensitivity. The loss of genes involved in chromatin structure and the metabolism of RNA conferred resistance to camptothecin is unexpected, given that both these processes have been implicated in DNA repair after damage[63,64]. Genes whose inactivation enhanced sensitivity to colchicine included those involved in the amino acid starvation response (DEPDC5 TSC1, SZT2 and NPRL2) and mRNA splicing (SNRPB2, SF3B2, PPIL1, RBM22 and DHX35), while mutation of genes that control vesicle trafficking (VPS16, VPS18, VPS29, VPS41, VPS51 and VPS52) or encode members of the Mediator complex (CCNC, CDK8 and MED26, MED1, MED7, MED12, MED18 and MED11) attenuated the cellular response to the drug. Unexpectedly, inactivation of genes encoding members of the TP53 signaling pathway (TFDP1 and HIPK2), SAGA H3 acetylation complex components

(KAT2A, TRRAP, TADA3, TAF5L, TADA2B, SGF29 and TADA1), and the Fanconi Anemia complex (FANCA, FANCC, FANCE, FANCF, FANCG, FANCL and FAAP100), all implicated in DNA damage repair, resulted in resistance to colchicine (Fig. 2E-2G). Sensitivity to palbociclib was enhanced in cells expressing sgRNAs targeting H4 acetylation, positive regulators of Pol II transcription and regulators of the DNA Damage Response pathway (Fig. 3A and 3B), although this sensitivity was much weaker than that seen with DNA damaging agents. This observation is consistent with long-term treatment with palbociclib inducing DNA damage, as has been suggested by a number of recent publications[65,66]. Unexpectedly, Metascape analysis of our palbociclib chemogenetic screen revealed that sensitivity to palbociclib was enhanced when genes involved in chromatin organization were targeted (Fig. 3A). Inactivation of members of the SIN3 histone deacetylase (SIN3B, SINHCAF and ARID4B), the NuA4 histone acetyltransferase (ING3, DMAP1, MORF4L2, YEATS4 and VPS73), the STAGA histone acetyltransferase (KAT2A,TADA1, TADA2B, TAF5L, and SUPT20H) and the Mediator (MED13, MED25, MED10, MED15, TAF7, TAG13 and CCNC) complexes all resulted in palbociclib sensitivity. (Fig. 3B). Each of these protein complexes promotes gene expression, suggesting that palbociclib sensitivity might be a result of a reduction in the transcription of genes important for the G1/S transition.

Because mechanisms of clinical resistance to palbociclib is an area of active investigation, we turned our attention to focus on these pathways. Metascape analysis of genes whose loss conferred palbociclib resistance were highly enriched for splicing factors, oxidative phosphorylation and mitochondrial translation, in addition to chromatin modification (Fig. 3A). STRING analysis of the high-confidence, physical interactions of proteins important for palbociclib sensitivity revealed multiple highly-connected interaction networks (Fig. 3B). Strikingly, almost 25% (170 out of the 689) of the genes whose mutation conferred unique resistance to palbociclib have terms associated with mitochondrial respiratory chain complex assembly, ATP synthesis or mitochondrial gene expression. Specifically, we see many components implicated in assembly of Mitochondrial Respiratory Chain Complex I and IV, as well as core mitochondrial ribosome and mitochondrial translation initiation and termination (Fig. 3A-3C). To confirm this positive genetic interaction between mitochondrial homeostasis and resistance to palbociclib, and to dissect whether specific electron transport chain steps might be implicated in this resistance, we asked whether chemical inhibition of oxidative phosphorylation could rescue sensitivity to palbociclib. To target different stages of the oxidative phosphorylation, we employed Rotenone, TTFA and Oligomycin, which inhibit Complex I, Complex II and ATP synthase, respectively. Cells were grown in the presence of palbociclib alone or in combination with each drug for 48 hours and viability was determined by PrestoBlue assay. Cells exposed to Rotenone, TTFA and Oligomycin all showed positive, suppressive growth interactions with palbociclib (Fig. 3D). While alternative explanations could explain the observed novel chemical-genetic interactions we uncovered here, such as either changes in phenotypic lag rates due to alterations in protein stability or more general screen variability[67], these results suggest a connection between mitochondrial gene function and CDK4/6 inhibitors.

Polycomb Repressive Complex Components Display Differing Responses to Palbociclib Treatment

Intriguingly, inactivation of EZH2, SUZ12 and EED, the three core members of the PRC2 complex, resulted in profound resistance to palbociclib, being the 8th, 4th and 3rd strongest resistance hits out of the 18,053 genes examined when ranked by the score of differential effect (Fig. 4A, Table S1). Mutation of RBBP7, which associates with the core PRC2 complex[20] along with a number of histone deacetylases[68], also desensitized cells to palbociclib, but to a more modest extent. Satisfyingly, inactivation of RING1, RNF2, and PCGF6, which are members of PRC1, also displayed resistance to palbociclib. The PRC1 complex contains a ubiquitin ligase that works in concert with PRC2 through H2AK119ub1 deposition, a histone mark that influences both PRC2 chromatin localization and catalytic activity[30,32]. As expected, PRC1 and PRC2 components identified in our palbociclib chemogenomics screen formed a highly interconnected STRING physical interaction network (Fig. 4B), indicating that loss of either H3K27me3 or H2AK119ub1 reduced sensitivity to this drug. In contrast, inactivation of genes encoding OGT, ASXL1 and HAT1, which are members of the H2AK119ub1

deubiquitinase complex that opposes PRC2-mediated gene repression[69], resulted in sensitivity to palbociclib (Fig. 4A). Importantly, no component of any PRC1 or PRC2 core complex displayed significant resistance or sensitivity to camptothecin and colchicine in our chemogenomics screens (Fig. 4C), implicating PRC2 in the regulation of G1 specifically, and not to other phases of the cell cycle or the DNA damage response pathway. PR-DUB components ASXL1 and OGT did show resistance to camptothecin, consistent with their role in repressing the homologous recombination DNA repair pathway[70]. We sought to confirm the role of the core PRC2 complex in palbociclib resistance by treating cells with combinations of palbcociclib and the EZH2 inhibitor GSK126 using a quantitative Crystal Violet assay. After nine days of drug combination treatments, we found that cells treated with increasing doses of GSK126 withstood palbociclib-induced growth suppression (Fig. 4D), confirming that inactivation of the PRC2 core complex, either through genetic inactivation or chemical inhibition, resulted in resistance to palbociclib.

The PRC2 core binds to auxiliary proteins to create biochemically distinct subcomplexes, termed PRC2.1 and PRC2.2[23,24]. These alternative complexes are thought to modify the chromatin localization and enzymatic activity of PRC2, reenforcing existing H3K27me3 in certain contexts[71–73], while initiating H3K27me3 deposition at new loci in others[33,39]. Mutation of the PRC2.1 complex members PHF1, MTF2, PHF19 and EPOP/C17orf96 all display significant resistance to palbociclib, with MTF2 being the strongest of these (Fig. 4A, 4C). Conversely, targeting the genes encoding the PRC2.2-specific accessory proteins AEBP2 or JARID2 resulted in enhanced or neutral palbociclib sensitivity, respectively. These data suggest that PRC2.1 plays a previously uncharacterized role in promoting G1 progression, while PRC2.2 antagonizes it. To confirm the results from our palbociclib chemogenomics screen, we generated polyclonal knockout mutant pools of the individual core and accessory proteins of PRC2. We generated these populations by independently infecting three distinct sgRNAs targeting genes for each PRC2 complex member, or positive and negative control genes, in GFP-positive and doxycycline-inducible Cas9 cells and induced DNA cleavage for three days (henceforth referred to as pooled knockouts). We performed Western blots to confirm reduction in protein levels for the genes targeted by the sgRNAs used to generate our pooled knockouts (Fig. S2B). After confirming reduction in the targeted proteins, we carried out a competitive growth assay using these pooled knockouts (schematic in Fig. S2A or see[51]). Briefly, GFP-positive pooled knockouts were mixed with GFP-negative wild-type cells and propagated in the presence or absence of palbociclib. The ratio of GFP-positive to GFP-negative cells was recorded every three days by flow cytometry for eighteen days. Pools containing sgRNAs against EZH2, SUZ12, EED and MTF2 all displayed resistance to palbociclib, similar to the level observed with sgRNAs targeting RB1, our positive control for palbociclib-induced growth defects (Fig. 4E). Conversely, compared with the dramatic reduction seen in pools transduced with CCNE1 sgRNAs, our positive control for enhanced palbociclib sensitivity CCNE1, sgRNAs targeting PRC2.2 components showed a slight, but statistically signification reduction in proliferation in palbociclib over the eighteen day assay (AEBP2: p-value = 0.002 and JARID2: p-value = 0.0148, unpaired two-tailed Student's t-test). Thus, we confirmed the results of our chemogenomics screen that MTF2-containing PRC2.1 inhibits G1 progression, while PRC2.2 does not, and could in fact promote it.

To further interrogate the role of PRC2.1 and PRC2.2 in the regulation of G1 progression, we generated SUZ12, MTF2 and JARID2-null monoclonal cell lines (which we will refer to as SUZ12Δ, MTF2Δ and JARID2Δ). We chose to mutate MTF2 to probe the function of PRC2.1, as it has been shown to be more highly expressed and the predominant PCL subunit associated with the PRC2 core complex in a variety of contexts[74,75]. Furthermore, we selected SUZ12 for inactivation out of the core PRC2 complex members, and not the catalytic subunit EZH2, because the presence of the EZH2 paralogue EZH1 might compensate for loss of EZH2[76]. Additionally, SUZ12 has a critical role in bridging accessory proteins with the catalytic core in all known PRC2 complexes[39]. MTF2Δ cells displayed resistance to palbociclib when compared with wild-type cells in a nine-day quantitative Crystal Violet assay (MTF2Δ IC_{50} = 1.033μM , wild-type IC_{50} = 0.3936μM) while JARID2Δ cells were slightly more sensitive than wild-type (JARID2Δ IC_{50} = 0.2216μM) (Fig. 4F). In addition

to showing sensitivity to palbociclib, MTF2Δ cells also displayed resistance to, ribociclib and abemaciclib, two CDK4/6 inhibitors that are structurally related to palbociclib, in a competitive growth assay (Fig. S2C). These results confirmed our screen results that mutation of MTF2 leads in CDK4/6 inhibitor resistance with verified clonal mutants.

Palbociclib exerts its chemotherapeutic effects by inducing a G1 arrest and senescence in tumor cells with a functional RB-E2F pathway[77–79]. However, a recent report demonstrates that palbociclib treatment induces both G1 arrest and apoptosis through the increase in DNA damage in cultured cells[80], introducing the possibility that PRC2.1 could be altering regulators of the DDR pathway, resulting in the observed palbociclib resistance. To determine if inactivation of PRC2.1 or PRC2.2 altered cell cycle progression, we examined how wild-type, SUZ12Δ, MTF2Δ and JARID2Δ cells responded to palbociclib-induced G1 arrest. To assess this directly, we performed a BrdU incorporation assay by growing each mutant for 24 hours in palbociclib, pulsed the cells with BrdU for one hour prior to harvest and then measured BrdU incorporation by flow cytometry. Each of the four cell lines had similar levels of BrdU incorporation in the absence of drug (Fig. 4G). However, MTF2Δ and SUZ12Δ mutants showed significantly more cells than wild-type in S-phase in the presence of palbociclib (Fig. 4G). JARID2Δ mutants showed fewer cells in S phase, but our assay was unable to establish that this reduction was statistically significant. To rule out the possibility that cellular viability was not compromised in our monoclonal knockout cell lines, we used Western blotting to monitor changes in PARP cleavage or increased BCL2L11/BIM expression, which both serve as apoptosis indicators[81]. There was no detectible basal increase in apoptosis in the monoclonal knockout mutant cell lines or when cells were treated with palbociclib for 48 hours, (Fig. S2D), supporting the conclusion that the resistance to palbociclib observed in the MTF2Δ and SUZ12Δ cells was due to the repressive role the MTF2-containing PRC2.1 complex plays in the canonical CDK4/6-RB1-E2F pathway.

PRC2.1 and PRC2.2 Mutants Display Altered H3K27me3 and Transcriptional Landscapes

To determine why the mutation of PRC2 subcomplex components altered the cellular response to palbociclib, we sought to see how H3K27me3 levels and gene expression changed in MTF2Δ and JARID2Δ cells. Western blotting of total H3K27me3 levels in three independently-generated clones indicated that there was no change in the bulk levels of H3K27me3 (Fig. 5A), suggesting that any change of phenotype observed in the mutants was due to a change in the localization of this mark and not due to an overall reduction in its abundance. This is in contrast to SUZ12Δ cells, which displayed a significant reduction in the H3K27me3 mark (unpaired Student's t-test, p-value = 0.0104). To probe the changes in transcription and H3K27me3 distribution genome-wide, we generated CUT&RUN libraries with an anti-H3K27me3 antibody and RNA-Seq libraries from total RNA isolated from our MTF2Δ and JARID2Δ cell lines, grown either in the presence or absence of palbociclib for 24 hours. Changes in H3K27me3 levels and mRNA expression were determined by comparing the enrichment of reads in the MTF2Δ and JARID2Δ libraries to the wild-type cell line (Tables S3 and S4). Because cancer cells have been known to adapt to palbociclib treatment partially through changes to histone marks, chromatin structure and gene expression[82–85], we also investigated how both transcript levels and H3K27me3 distribution responded to treatment with palbociclib in our clonal knockout cell lines. Primary component analysis (PCA) of our called, reproducible H3K27me3 peaks and transcript abundance from our CUT&RUN and RNA-seq data, respectively, showed a high percentage of variance between each of the genotypes tested, along with good clustering of repeats of the same genotype and treatments (Fig. S3A), suggesting a shift in the epigenetic and transcriptional landscapes when either MTF2 or JARID2 are absent. PCA analysis of our RNA-Seq experiment revealed substantial shifts in variance between palbociclib-treated and Mock-treated samples for each genotype (Fig. S3A, bottom), suggesting that exposure to palbociclib resulted in changes in gene expression, consistent with previous reports[86,87]. However, the PCA of our CUT&RUN experiment did not reveal large differences in H3K27me3 distribution between palbociclib-treated and untreated samples (Fig. S3A - top). In line with this observation, when we analyzed the change in distribution of H3K27me3 peaks between palbociclib and Mock treated cells using DESeq2, we found no

significant changes in the location of H3K27me3 reproducible peaks in the presence or absence of palbociclib (data not shown). This suggests that MTF2Δ mutants are not resistant to palbociclib because MTF2 is required for a transcriptional adaptation to the drug, but instead because MTF2 alters expression of genes important for G1/S progression, even in unperturbed cells.

Due to the known role of PRC2 in repressing gene expression, we next asked how H3K27me3 distribution changed in promoters of genes. We defined promoters as 4kb upstream and 1kb downstream of all annotated transcription start sites, and calculated the total number of reads within each of these regions. Our parameters led to ~61,000 genomic regions being designated as promoters. In addition to annotated protein coding genes, this included the promoters of non-coding transcribable units such as rRNA, miRNAs, lncRNAs, and pseudogenes. We observed a greater number of promoters with significantly decreased H3K27me3 ($\log_2$ fold-change ±1, adjusted p-value < 0.1) in the MTF2Δ compared to JARID2Δ cell lines (5,808 vs 1,034 promoters, respectively). Of these, 5,149 promoters displayed MTF2-dependent H3K27me3, 392 were JARID2-dependent and 629 were co-dependent on MTF2 and JARID2 for wild-type levels of H3K27me3 (Fig. 5B and 5D). Consistent with the greater change in H3K27me3 signal at promoters in MTF2Δ cells, 733 vs 114 transcripts were significantly upregulated upon MTF2 vs JARID2 inactivation, respectively, with 666 transcripts that were exclusively MTF2-dependent, 47 transcripts that were exclusively JARID2-dependent, and 67 transcripts displaying co-dependence on both MTF2 and JARID2. These results indicate that the MTF2-containing PRC2.1 complexes affect the deposition of H3K27me3 in the promoter regions of more genes than the JARID2-containing PRC2.2, and therefore, are more important for transcriptional repression in HAP1 cells.

Given the diverse regulatory roles of PRC2 in different biological contexts, and the limited information on PRC2.1 and PRC2.2 outside of stem cells, we were curious to see what classes of genes were being differentially regulated in the MTF2Δ and JARID2Δ cell lines. Only ~30-40% of the promoters with significantly changed levels of H3K27me3 were upstream of protein coding genes (Fig S3B), while ~80-90% of the significantly differentially expressed transcripts encoded proteins (Fig. S3C). Therefore, we focused a Metascape analysis on the promoters and mRNAs of protein coding genes with differential H3K27me3 and transcript levels, respectively (Fig. 5C). Analysis of the promoters of genes with decreased H3K27me3 and increased transcript levels in both MTF2Δ and JARID2Δ lines were terms associated with embryonic morphogenesis, cell fate commitment and developmental growth, all processes previously been shown to be regulated, at least in part, by PRC2[88].Intriguingly, terms for genes that specifically displayed decreased promoters H3K27me3 and upregulated mRNA in MTF2Δ cells included the pro-growth pathways cGMP and ERBB4 signaling. Conversely, terms for genes which displayed increased promoter H3K27me3 signal and decreased transcript levels in JARID2Δ cells contained pathways that could reduce cellular proliferation and viability, such as positive transcriptional regulation of RUNX1 and positive regulators of program cell death. We also saw terms that had opposite effects on H3K27me3 and transcript levels in MTF2Δ compared to JARID2Δ cells, such as secretion by the cell and regulation of cellular component biogenesis, which could potentially exacerbate palbociclib-induced growth defects[89,90]. Together, these data support the notion that MTF2 antagonizes cell growth in normal cellular conditions, while JARID2 promotes it.

PRC2.1 and PRC2.2 Mutants Display Differential H3K27me3 Modification in Promoters in Cell Cycle Related Genes with CpG Islands

MTF2-containing PRC2.1 have been previously shown to localize to chromatin using a winged helix in its extended homology domain that has affinity for CG-rich sequences[28,29], whereas PRC2.2 localization is dependent on chromatin context, specifically H2AK119ub1 deposited by PRC1[31–33]. To determine whether CpG island targeting by PRC2.1 could help explain the palbociclib resistance we observed in the absence of MTF2, we identified and plotted 1,877 peaks that overlapped with CpG islands in wild-type cells and had the greatest H3K27me3 signal in a 10kb window surrounding the CpG islands. We then plotted the H3K27me3 signal observed in the MTF2Δ and JARID2Δ cells for these same loci (Fig. 5E). We observed a complete loss

of H3K27me3 signal intensity at CpG islands in the MTF2Δ mutants, but only a partial loss at these loci in JARID2Δ cells (Fig. 5E and Fig. S3D). When we expanded our findings genome-wide, we found a significant loss of H3K27me3 peaks at CpG islands in MTF2Δ cells (Fisher's exact test, odds ratio = 20.4, p-value $2.2x10^{-308}$), compared with JARID2Δ, where this loss was much more modest (fisher's exact test, odds ratio = 9.8, p-value = $6.5x10^{-7}$). This result is consistent with the interpretation that the MTF2-containing PRC2.1 is required for all H3K27me3 deposition at CpG islands, whereas JARID2-containing PRC2.2 is only required to achieve full wild-type H3K27me3 levels at these sites.

CpG islands are a very common feature of mammalian promoters, with 50-70% human promoters estimated to contain at least one CpG island[91]. Since promoters are highly associated with CpG islands, we examined 2,000 promoters with the highest level of H3K27me3 signal intensity that overlapped with CpG islands in wild-type cells, then plotted the H3K27me3 signal intensity at those same loci in our mutant cell lines (Fig. 5F, left plots). Consistent with the result seen at CpG islands genome-wide, we observed a complete loss of high signal intensity in the MTF2Δ cells, but only a slight loss in JARID2Δ cells. When we averaged the H3K27me3 signal intensity over all 25,124 promoters that contain CpG islands, we observed a pattern of MTF2Δ cells having greatly decreased H3K27me3 levels in these regions, particularly surrounding the transcription start site (Fig. 5F, right plot). We also observe a partial loss of H3K27me3 at the 2,000 promoters that contain CpG islands with the greatest intensity of H3K27me3 in the JARID2Δ lines compared to wild-type (Fig 5F, left plots), in line with what was seen at CpG islands genome-wide. However, when we averaged the signal intensity over all 25,124 promoters that contain CpG islands in JARID2Δ cells, the distribution of H3K27me3 in the promoter regions looks similar to the wild-type distribution (Fig. 5F, right plot). Reactome and MSigDB analysis of the promoters of protein coding genes that overlapped with CpG islands showed strong enrichment for terms associated with cell cycle and E2F target genes (Fig. 5G) as well as enrichment binding E2F6 (Fig. S3E, p-value: $1.9x10^{-91}$), which both regulates transcription of G1 progression genes[92] and is a well characterize component of Polycomb complexes[23,93]. These results suggest that MTF2 is required for H3K27me3 deposition at promoters containing CpG islands involved in cell cycle regulation and can explain why MTF2Δ cells display a greater change in gene expression than do JARID2Δ cell lines.

PRC2.1 Represses Expression of CCND1 and CCND2

Our CUT&RUN results suggest that MTF2-containing PRC2.1 impacts gene expression, at least in part, through deposition of H3K27me3 at promoters with CpG islands. Therefore, we hypothesized this PRC2 complex must be antagonizing G1 progression through repression of cell cycle-promoting genes. When inspecting the results of our CUT&RUN and RNA-Seq experiments, we found that the promoters of both CCND1 and CCND2 had lost H3K27me3 signal (Fig. 6A) and displayed strong transcriptional induction in MTF2Δ cells (Fig 6B). In fact, while CCND1 and CCND2 were both among the most up-regulated statistically-significant transcripts within the MTF2Δ cell line, their transcription and promoter H3K27 methylation were unaltered in JARID2Δ cells (Fig. S4A and S4B). Furthermore, CCND1 and CCND2 displayed both decreased H3K27me3 and increased mRNA levels in MTF2Δ cells (Fig. 6C), suggesting that the increase in these transcripts was due directly to a change in H3K27me3 in their promoters. Given that increased CCND1 levels is sufficient to drive increased CDK4/6 kinase activity, upregulation of these D-type cyclins is likely to be a significant contributor to the palbociclib resistance in MTF2Δ cells. DESeq2 analysis of H3K27me3 density in MTF2Δ cells displayed a statistically significant 4.3 and 2.7 log_2 fold-decrease in H3K27me3 signal in the promoter region of CCND1 and CCND2, respectively, when compared to wild-type H3K27me3 levels (Fig. 6D, Table S3), whereas changes in H3K27me3 levels in the CCND3 promoter were not statistically significant (Fig S4D, Table S3). Given our observation that H3K27me3 signal is lost at CpG islands in MTF2Δ cells, we inspected the D-type cyclin promoters for CpG islands. Indeed, the regions upstream of all three D-type cyclins contained CpG islands, but CCND1 and CCND2 had regions of GC density about seven times larger (7,460bp and 6,003bp, respectively) than CCND3 (996bp). Furthermore, the promoter of CCND1 contained about twice as many CpG repeats than did CCND2 (575 vs 379) and about six times as many CpG repeats as CCND3 (575

vs 95) (Fig. S4D). These results suggest that the levels of CCND1 and CCND2 mRNA transcripts, but not CCND3, were regulated by MTF2 in a CpG island-dependent manner.

We sought to confirm our observation that ablation of MTF2 resulted in increased levels of CCND1 and CCND2 protein. We generated pooled knockouts of MTF2, JARID2 and the core PRC2 components SUZ12, EZH2 and EED using three independent sgRNAs. In pooled knockouts of MTF2, EZH2, EED and SUZ12, we observed an increase in both CCND1 and CCND2 protein levels by Western blot, but not for CCND3 (Fig. 6E). Consistent with the results from our CUT&RUN and RNA-Seq datasets, we did not observe a significant change in either CCND1 or CCND2 levels in JARID2 pooled knockouts. We next examined mRNA and protein levels of the D-type cyclins in MTF2Δ and JARID2Δ clones by qRT-PCR and Western blotting, respectively. Again clonal knockouts of SUZ12Δ and MTF2Δ, but not JARID2Δ lines, had increased mRNA (Fig. 6F) and protein levels (Fig. 6G and Fig. S6E) for both CCND1 and CCND2, but not CCND3. To determine whether other genes involved in the canonical CDK4/6-RB-E2F pathway were also altered, we examined mRNA and protein levels of known cell cycle regulators in our knockout cell lines. In contrast to CCND1 and CCND2, none of the E-type cyclins, CIP/KIP CDK inhibitors, RB1 or E2F proteins displayed significantly altered mRNA transcript abundance in our RNA-seq experiment in either MTF2Δ or JARID2Δ lines (Fig. S4F). To confirm that protein stability of these factors was not altered in our knockout lines, we also examined protein levels of a panel of known G1 regulators by Western blot (Fig. S4G). Similarly, we did not observe an increase in levels of any of the tested proteins, confirming that CCND1 and CCND2 were the only up-regulated canonical CDK4/6-RB-E2F pathway regulators in MTF2Δ cells.

While D-type cyclins are necessary to activate the kinase activity of CDK4/6, they have also been shown to play roles outside of the RB1-E2F pathway[87–89]. We sought to test if CDK4/6 activity was increased in MTF2Δ. To do this, we determined the extent of RB1 phosphorylation at S807/S811, which are well-characterized CDK4/6 targeted residues. To do this, we titrated wild-type, MTF2Δ, and JARID2Δ cells with increasing amounts of palbociclib and determined the levels of total RB1 and phosphorylated RB1 levels to calculate the ratio at each concentration. In each of our cell lines, higher concentrations of palbociclib resulted in decreased levels of phosphorylated RB1, as expected. However, compared to WT or JARID2Δ cells, MTF2Δ mutant cells maintained a higher ratio of phosphorylated to unphosphorylated RB1 at each concentration of palbociclib tested (Fig. 6H). This result suggests that the increased levels of CCND1 and CCND2 in MTF2Δ cells increases CDK4/6 kinase activity, driving cells into S-phase (Fig. 4G). In total, our results suggest that MTF2-contiaing PRC2.1 antagonizes G1 progression by repressing expression of the D-type cyclins CCND1 and CCND2.

Discussion

Regulated progression through cell cycle phases is critical to normal cellular function and viability, while disordered progression is the hallmark of many disease states. Although the cell cycle has been an area of active research for decades, our understanding of its regulation remains incomplete. Using a chemogenetic approach, we found that inactivation of members of PRC2.1, but not factors specific to PRC2.2, resulted in profound resistance to the CDK4/6 inhibitor palbociclib. Loss of PRC2.1 complex members led to upregulation of the D-type cyclins CCND1 and CCND2, resulting in increased RB1 phosphorylation and S-phase entry in palbociclib-treated cells. We propose that PRC2.1, but not PRC2.2, meditates H3K27me3 deposition in the promoters CCND1 and CCND2 through the recognition of the CpG islands. These results tie PRC2.1 directly to the regulation of G1 progression.

In the chemogenomic screens reported here, we recovered genes in a diverse array of biological pathways that resulted in sensitivity or resistance to well-characterized cell cycle inhibitors. In addition, we observed that inactivation of genes involved in mitochondrial homeostasis resulted in resistance to palbociclib. Small molecule inhibitors of EZH2 or the electron transport chain co-administered with palbociclib resulted in enhanced cell growth (Fig. 3D and 4D), supporting the observed chemical-genetic interaction seen in our screen. However, genes identified in genetic screens should be interpreted with caution. Reproducible, and

sometimes robust interactions can sometimes result from complicated changes in doubling time or alterations to the physiologic state of the cell[61]. It was recently demonstrated that genes encoding members of the electron transport chain are over-represented in DepMap co-dependency data, due to the remarkable stability of these protein complexes, which results in phenotypic lag that can vary in different backgrounds[61]. While mitochondrial complex assembly factors as enriched in Metascape analysis of our camptothecin screen as well as in palbociclib (Fig. 2C), the enrichment was greater than 1600-fold more significant in palbociclib (Fig. 3A). Moreover, a number of reports have found increased oxygen consumption and ROS production due to greater number and size of mitochondria in cells treated palbociclib[82,83,90]. This is consistent with a direct effect of CDK4/6 activity on mitochondrial function. Thus, in the case of both the PRC2 and the mitochondrial gene cluster, our data and that of others suggest that these results represent a direct link between these pathways and CDK4/6 biology.

Recently, PRC2 subcomplex accessory proteins have been implicated in an increasing number of processes that define cellular identity, including stem cell maintenance, differentiation and cancer[35,36,91,92]. Despite the importance of controlled cellular division to each one of these processes, few reports have interrogated the roles of the different subcomplexes outside of stem cell model systems or specifically on their role in cell cycle regulation. Here, we show that cells that lose either MTF2 or SUZ12 continue to proliferate despite palbociclib blockade (Fig. 4E and 4G). These mutants show no apparent change in the proportion of cells undergoing apoptosis and display a greater proportion of cells entering S-phase in the presence of palbociclib, compared to wild-type or JARID2Δ cells. This increase is consistent with our findings that in MTF2Δ cell lines treated with palbociclib, a higher percentage of RB1 remains phosphorylated, while a similar increase is not seen in JARID2Δ cells. We surmise that the upregulation of CCND1 and CCND2 expression observed in cells lacking MTF2 results in increased CDK4/6 kinase activity that is sufficient to overcome palbociclib-mediated inhibition. Critically, we did not observe any significant changes in expression of other classic regulators of the CDK4/6-RB1-E2F pathway in either our CUT&RUN or RNA-Seq datasets (Fig. S4F and S4G). While we cannot exclude the possibility that MTF2 inactivation alters the expression of other factors that influence G1 progression, we propose CCND1 and CCND2 represent major targets of PRC2.1 repression restraining G1 progression in HAP1 cells. Though a recent report demonstrated that low MTF2 expression leads to increased chemotherapeutic resistance in leukemia[93] and down regulation of MTF2 was correlated with poorer clinical outcomes in breast cancer[94], more work is needed to determine whether D type cyclins are the critical PRC2.1 targets in tumors themselves.

Work over the past decade has implicated accessory proteins as critical for proper genomic localization of the PRC2 enzymatic core. However, reports differ on in what chromatin and cellular contexts these subcomplexes act. Data from both mouse and human ES cells has suggested that PRC2.1 and PRC2.2 have overlapping genomic occupancy[65,67], and that either subcomplex alone is capable of maintaining pluripotency[65,67,95]. However, recent reports have found differing dependencies on these subcomplexes for proper distribution of H3K27me3 in cellular models of differentiation[27,33,96–98]. For example, a recent study in a model of induced differentiation suggested that MTF2 is involved in the maintenance of repression of PRC2 genes, whereas JARID2 is important for de novo deposition of H3K27me3 critical for gene silencing through genes “pre-marked” with H2AK119ub1[33]. Conversely, PRC2.1 was shown to be required for the majority of H3K27me3 deposition during induced cell-fate transitions in mESCs, whereas PRC2.2 was not[27]. This study generated a triple knockout of all three PCL proteins (PHF1, MTF2 and PHF19), resulting in complete ablation of all PRC2.1 activity and did not probe the contribution of each accessory protein individually. Furthermore, MTF2 transcript levels are down regulated upon differentiation, whereas PHF1 and PHF19 levels increase[99]. These data suggest that the subunit composition of PRC2.1 changes during this process. In our experiments, MTF2 is the only PCL subunit important for D-type cyclin repression. These data are consistent with cell type-specific contributions of this class of proteins.

Using mutants of genes encoding subunits specific to either PRC2.1 or PRC2.2, we investigated the role of each subcomplex in cell cycle progression in HAP1 cells. In contrast to what has been demonstrated for ES cell lines where the two subcomplexes work synergically at the majority of sites[65,67], we show that MTF2 is required for the majority of H3K27me3 deposition at CpG islands genome-wide and JARID2 was only partially required for H3K27me3 at these loci (Fig. 5E). Importantly, the presence of MTF2 is more critical than JARID2 for the accumulation of H3K27me3 directly upstream of annotated transcription start sites in CpG islands-containing promoters in HAP1 cells (Fig. 5F). Concordant with the patterns in H3K27me3 in promoters, we found that MTF2 loss resulted in a greater number of upregulated transcripts than JARID2 loss (Fig. 5B and Fig. S3C). Finally, MTF2Δ cells displayed a stronger correlation between genes with decreased promoter H3K27me3 levels and increased transcription than did JARID2Δ lines (Fig. 6C and Fig. S4C). However, we cannot exclude the possibility that AEBP2 plays a larger role in the activity of PRC2.2 than does JARID2 in these cells, as we identified AEBP2 as significantly, albeit modestly, increasing sensitivity to palbociclib in pooled knockout cells (Fig. 4A and Fig. 4E). As H3K27me3 peak distribution was altered in the JARID2Δ cell lines (Fig. S3A), loss of JARID2 could alter H3K27me3 sites distal to promoters to change chromosome architecture or enhancer-promoter interactions. Alternatively, genes upregulated by loss of either MTF2 or JARID2 which did not have a significant alteration in promoter H3K27 methylation could be indirect effects. A recent report found that while PRC2.2 activity was not required for establishment of H3K27me3 during differentiation, but was instead required for recruitment of a PRC1 complex required for higher level chromatin interactions[27]. Future studies will be necessary to fully understand the coordination between these complexes.

The efficacy of CDK4/6 inhibitors in the treatment of HR+/HER2- breast cancer demonstrates the success of applying basic knowledge of cell cycle regulation to the generation of clinically-relevant drugs. However, despite this success in the treatment of breast cancer, the efficacy of CDK4/6 inhibition is variable, with 10-20% of tumors primarily resistant and an additional 40% becoming resistant to these drugs within the first two years[100,101]. Moreover, CDK4/6 inhibitors are currently being explored for other tumor types, and these are each likely to have novel resistance mechanisms[92,102,103]. Thus, understanding perturbations in molecular pathways that can result in resistance to CDK4/6 inhibition could lead to improved patient responses and outcomes. In this study, we found that mutation of the PRC2.1 accessory protein MTF2 results in the development of resistance to palbociclib-induced proliferation reduction. Previously, EZH2, SUZ12, EED, MTF2 and JARID2 have all been suggested to not only act as oncogenes[104–111], but also to have tumor suppressor activities[30,91,93,94,112–114], depending on the type of cancer. These observations not only underscore the context-dependent ramifications of mutation of these PRC2 complex members, but also may help inform the context in which CDK4/6 inhibitors are most efficacious. Clinical trials using CDK4/6 inhibitors in combination with other therapeutics are underway and the mutational status and expression levels of PRC2 subunits might serve as predictors of efficacy.

Acknowledgments

I would like to thank the members of the Toczyski, Jura, Ramani and Shen lab for their experimental and intellectual feedback on the preparation of this manuscript. I would specifically like to thank Hiten Madhani and Natalia Jura for their thoughtful discussions on this project and for mediating collaborations critical in completion of this work. Additionally, I would like to thank Nerea Sanvisens Delgado for initial compound dosing used in this study and Sarah Elmes for support in developing our flow cytometry experiments. This work was supported by an NIH grants (R35 GM118104 to David Toczyski and (R01AG057497, R01EY027789, UM1HG009402 and U01DA052713 to Yin Shen). DNA sequencing was performed at the UCSF Center for Advanced Technology, and flow cytometry and qRT-PCT at UCSF Laboratory of Cell Analysis.

Lead Contact and Materials Availability

Requests for further information and reagents should be directed to and will be fulfilled by the Lead Contact, David Toczyski (dpt4darwin@gmail.com).

Methods

Cell Lines

Cas9 expressing HAP1 cells were cultured in IMDM supplemented with 4mM glutamine (Gibco), 10% Tetracycline-free FBS (Sigma-Aldrich) and either 1x Antibiotic, Antimycotic (Invitrogen) or 1% penicillin-streptomycin (Sigma-Aldrich). HAP1 cells stably expressed Cas9 were employed for the whole-genome screen, while for subsequent experiments, a HAP1 line harboring a doxycycline-inducible Cas9 was utilized. HEK293T cells used for the production of virus were cultured in DMEM supplemented with 2mM glutamine (Gibco), 10% Tetracycline-free FBS (Sigma-Aldrich) in 1x Antibiotic, Antimycotic (Invitrogen). Cells were detached from tissue culture dishes using 0.25% Trypsin (Gibco) and maintained at 37˚C, 5% CO2. Our laboratory conducts regular mycoplasma testing of cultured cells with the MycoAlert Mycoplasma Detection kit (Lonza), and no mycoplasma contamination of any cell line was detected during this study.

Genome-wide chemical screening

The lentiviral TKOv3 sgRNA library (Addgene #90294) was used to perform pooled genome-wide CRISPR knockout screens. The library contains 70,948 guides, targeting 18,053 protein-coding genes (4 guides/gene). Ninety million HAP1 cells stably expressing Cas9 were seeded into 15cm dishes and infected with TKOv3 lentivirus at a multiplicity of infection of roughly 0.3, such that every sgRNA is represented in approximately 200-300 cells after selection (>200-fold coverage). After 24 hours of infection, cells with successful viral integration were selected in 25mL IMDM medium containing 1μg/mL puromycin (Sigma-Aldrich). Selection took place for 48 hours. Following selection, cells were harvested, pooled, and split into 3 replicates of 15 million cells each to maintain >200-fold coverage of the sgRNA library (day 0). At day 3, each replicate was split such that every drug screen had a at least 15 million cells per replicate to maintain >200-fold coverage. The drug concentrations (IC_{30}-IC_{50} determined as described below) used in the genome-wide chemical screens were as follows: Palbociclib - 0.7μM, Colchicine - 9.2nM, Camptothecin - 1nM. An increase in potency was observed for most drugs when used in the pooled screens, thus screening concentrations were adjusted to preserve IC_{30}-IC_{50} throughout each passage. Cells were subject to treatment with drug in 0.1% DMSO, or 0.1% DMSO alone. Drug- containing media was refreshed every 3 days, along with the passaging of cells and the collection of cell pellets. To preserve >200-fold coverage, 20 million cells were pelleted with every passage, from day 0 to day 18.

Genomic DNA extraction and sequencing library preparation were performed as described previously[53]. Briefly, genomic DNA from cell pellets were extracted using the Wizard Genomics DNA Purification Kit (Promega) and quantified using the Qubit dsDNA Broad Range Assay kit (Invitrogen). Sequencing libraries were prepared as described previously[122]. Briefly, two PCR amplification steps were performed to first enrich for the gRNA-regions in the genome and second, attach Illumina sequencing indices to the amplified regions. Sequencing libraries were prepared from 50μg of genomic DNA (200-fold library coverage) using the NEBNext Ultra II Q5 Polymerase (NEB). Primers used included Illumina TruSeq adapters with i5 and i7 indices. Barcoded libraries were gel-purified using the PureLink Quick Gel Extract kit (ThermoFisher) and sequenced on an Illumina HiSeq2500.

Drug concentrations for chemical screening

Drug dosing experiments were performed to determine screening concentrations. HAP1 cells stably expressing Cas9 were seeded at a density of 2.5 million cells per 15-cm dish. Cells were treated with 0.1% DMSO, or drug in 0.1% DMSO, 2 hours after seeding. Viable adherent cells were counted 2 days post-treatment on a Coulter counter, and inhibitory concentrations were determined. The following are ranges of drug

concentrations used in the dosing experiments: Palbociclib: 1.5-10μM, Colchicine: 1.5-150nM, Camptothecin: 1-5nM.

Orobas Pipeline for Scoring Chemical Genetic interactions

The Orobas pipeline (version 0.5.0 – Supplemental File 1) was used to score chemical genetic interactions from the genome-wide CRISPR/Cas9 screen data. The process is summarized here, and the complete R code is provided as a supplemental file. sgRNAs were normalized to sequencing depth for each sample and the $\log_2$ fold change (LFC) in sgRNA abundance was calculated for each condition relative to the corresponding T0 sample. Guides with fewer than 30 read counts in the T0 sample were filtered out from further analysis, and genes with fewer than 3 remaining guides post-filtering were also filtered out from scoring. Residual effects were computed for each gene by calculating the residual LFC between sgRNAs in treated vs. DMSO samples after averaging technical replicate LFCs. Residual effects were then M-A transformed and loess-normalized to account for potential skew and non-linearity present in the data, and per-gene effect sizes and FDRs were computed by applying the moderated t-test to normalized residual effects. Hits were called as genes with FDRs less than 0.4 and per-gene effect sizes greater than 0.5 or less than -0.5 (a complete list of effect sizes and FDRs is included as Table S1).

STRING Interaction Network Generation

STRING networks were set to only display physical interactions scores that were returned with high confidence (0.7) and taken from text-mining, experiments and databases.

sgRNA Lentiviral Vector Cloning

Oligos for sgRNA targets were designed to contain the 5' overhang CACCG- for the sense oligo 5' and for that antisense 3' over hang AAAC- and -C, respectively. 10μM each of sense and antisense oligos (Integrated DNA Technologies) were mixed in 1x T4 DNA Ligase buffer and water to a total volume of 10μL. This mixture was heated to 95ºC for 5 mins, then oligos were annealed by decreasing the temperature at a rate of -0.1ºC/second till the mix reached 25ºC. Annealing reactions were diluted 1:10 with water and then 1μL was used to ligate into 100ng of BsmBI digested pLentiGuidePuro vector (Addgene #52963) in 1x T4 DNA Ligase Buffer. 600 units of T4 DNA Ligase (NEB) and water to a total volume of 25μL. After incubating for 1hr at 37˚C, 2μL of the ligation reaction was transformed into BME pre-treated XL10-Gold cells (Agilent) per the manufacturer's instructions and plated on LB + 100μg/mL carbenicillin plates for selection. Plasmids recovered from single colonies were confirmed by Sanger sequencing.

Polyclonal and Monoclonal Knockout Generation

Cas9 expressing HAP1 cells were transduced with pLentiGuidePuro vectors (Addgene #52963) expressing a single sgRNA (see Table S5 for sgRNA sequence). Lentiviral transduction was conducted at low MOI (~30%) following standard protocols. Integration of the sgRNA was selected with 1μg/mL puromycin for up to two days, followed by combined puromycin selection and Cas9 induction for three days with 1μg/mL doxycycline. This polyclonal pool of pLentiGuidePuro transduced cells was then used for "pooled" knockout experiments or used to generate monoclonal cell lines. Trypsinized, single cells were then sorted into individual wells in a 96-well plate using the Sony SH800 sorter (UCSF, LCA). Isolated single cell-derived colonies were screened for mutation by PCR, followed by Sanger sequencing of the purified PCR product and ICE analysis (Synthego) of the resulting chromatographs. Candidate clonal knockouts were then confirmed by Western blot. Only monoclonal lines that clearly displayed knockout alleles and had no protein product by Western blot were utilized further.

Competitive growth assays (GFP/BFP pooled knockouts and GFP+/monoclonal knockout pools)

For pooled knockout competitive growth assays, HAP1 cells harboring an inducible Cas9 and expressing GFP and HAP1 cells expressing BFP (Hundley et al.) were mixed at a ratio of 1:4 GFP:BFP HAP1 cells into a

single well, with three GFP/BFP cell mixtures for each gene targeted for inactivation. Mixtures were transduced at a low MOI with a pLentiGuidePuro vector expressing one sgRNA (three biological replicates per gene, sgRNAs in Table S5). After 24 hours of lentiviral transduction, pools of cells were selected with 1μg/mL puromycin for one day, followed by 1μg/mL puromycin and doxycycline for three days to select for sgRNA integration and to induce Cas9 expression. After three days of Cas9 induction, pools were split into media with or without palbociclib every three days, for eighteen days. The GFP/BFP ratio was monitored on the Attune NxT (Invitrogen) flow cytometer every three days. FlowJo v10 was used to determine the GFP/BFP ratio at each time point. The ratio of GFP to BFP was normalized to the day zero ratio (prior to splitting into palbociclib), and subsequently to the matched untreated ratio at each time point.

For HAP1 GFP+/– competitive growth assays, clonal MTF2Δ or JARID2Δ GFP- cells were mixed with HAP1 GFP$^+$ clones at 1:4 GFP-:GFP+ ratio, split into media with or without drug, and analyzed by flow cytometry as described above.

Western blotting

Harvested cell pellets were lysed in 1xRIPA buffer supplemented with 1x EDTA-free cOmplete protease inhibitor (Roche) and 1x PhosphoSTOP phosphatase inhibitor (Roche) for 30 minutes on ice with two rounds of 15 second vortexing. Lysates were cleared at 21,000 xg for 10mins at 4˚C. Protein concentration was determined by BCA assay and BSA standard curve (Pierce), and samples were adjusted to 1μg/μL total protein with 1xRIPA and SDS-PAGE sample loading buffer was added (62.5 mM Tris-HCl (pH 6.8), 2.5% SDS, 0.1% bromophenol blue, 10% glycerol, 5% β-mercaptoethanol (v/v)). 10μg of total protein was loaded per lane onto a 4-20% Criterion Tris-HCl Protein gel (Bio-Rad) and separated by electrophoresis at 150 V for 1hr. Proteins were transferred and immobilized onto a nitrocellulose membrane (GE Healthcare) by electrophoresis for 1h at 100V in standard transfer buffer containing 20% methanol. Membranes were blocked for an hour at room temperature and then then probed overnight in a 1:1000 dilution of 1˚ antibody (unless otherwise indicated) at 4˚C and in a 1:10,000 2˚ antibody at room temperature for 1hr at in the appropriate blocking buffer. Chemiluminescent and fluorescent signals were visualized with an Odyssey FC imager (LICOR).

Cell Cycle Analysis by Propidium Iodine

200,000 cells/well were plated in 6 well dishes at, as to be 10-20% confluent at the time of treatment. Cells were treated with inhibitors 24h after plating, then harvested 48h later by trypsinization, washed twice with cold 1x PBS, fixed by dropwise addition of ice-cold 70% ethanol, and incubated at 4˚C overnight. Fixed samples were washed twice with 1x PBS + 1% BSA prior to resuspension in a solution of 1x PBS, 1mg/mL RNase A and 50 μg/mL propidium iodide for 1 hour at 37°C. DNA content of at least 20,000 single cells was determined by Attune NxT flow cytometer (Invitrogen), and data were analyzed using FlowJo v10.

BrdU Incorporation Assay

250,000 cells/well were plated in 6-well dishes and grown for 24hrs prior to treatment. Cells were then treated with either DMSO (mock) or 1.5μM palbociclib for a total of 24hrs, with 10μM BrdU being added to the culture medium 1hr prior to harvesting. Cells were counted using the Countess automatic hemocytometer (Invitrogen) to ensure that only 1 million cells were stained. Cells were prepared for analysis using BD Pharmagen BrdU Flow Kits (BD Biosciences) according to the manufacturer's instructions. BrdU incorporation was determined for at least 20,000 single cells by Attune NxT flow cytometer (Invitrogen), and data were analyzed using FlowJo v10.

Quantitative Crystal Violet Proliferation Assay

1mL of a 1,000 cells/mL suspension were seeded into a per well in a 6-well plate containing 1mL IMDM supplemented with double the indicated concentration of palbociclib and GSK126 in technical triplicate. Cells were allowed to proliferate for nine days, with the media supplemented with the drug at the concentration

indicated replaced every three days. After nine days, cells were washed once with 1x PBS, followed by staining and fixation in a 0.25% Crystal Violet, 20% methanol solution for 10mins at room temperature. Following staining, cells were washed six times with 1x PBS and lysed in a 100mM sodium citrate and 50% ethanol solution for 30mins at room temperature on an orbital shaker. Lysates were recovered and absorbance at 590nM was detected using a Synergy Neo2 Microplate Reader (BioTek). Proliferation at each concentration was determined relative to untreated wells.

PrestoBlue Proliferation Assay

45μL of a 50,000 cells/mL cell suspension was seeded into a 96-well plate containing 45μL of IMDM supplemented with the indicated concentration of palbociclib, antimycin A, TTFA or oligomycin in triplicate. After proliferation for 48hrs, 10μL of PrestoBlue (Invitrogen) was added to each well and incubated for 30mins at 37˚C. Conversion of PrestoBlue was determined by recording the fluorescence excitation at 560nM and emission at 590nM using a Synergy Neo2 Microplate Reader (BioTek). Proliferation at each concentration was determined relative to untreated wells.

RNA-Extraction

150,000 cells were seeded into 6-well plates and allowed to grow overnight. Cells were treated with DMSO (Mock) or 1.5μM palbociclib for 24hrs prior to harvesting directly in TRIzol reagent (Invitrogen). After chloroform extraction, the aqueous phase was transferred to a fresh tube and 1 volume of 100% ethanol was added and mixed thoroughly before binding to an RNA Clean & Concentrator (Zymo). RNA was DNase I digested on-column (Zymo), purified according the manufacturer's instructions and eluted in]nuclease-free water. To prepare RNA-Seq libraries, 2μg of total RNA was polyA, followed by Illimina adaptor ligation and paired-end sequencing on an Illumina HiSeq at a depth of at least 22 million reads per sample by Azenta.

First Strand cDNA Synthesis and qRT-PCR

2μg of total RNA was first heat denatured in the presence of dNTPs and oligo-dT at 65˚C for 5mins. RNase inhibitor and Tetro reverse transcriptase (Bioline) was then added to heat denatured total RNA and cDNA was synthesized at 45˚C for 1hr, followed by heat inactivation at 85˚C for 5mins. cDNA synthesis reactions were then diluted 1:5 and 2μL was added into qRT-PCR reaction mix, utilizing SensiFast Lo-ROX qRT-PCR Mastermix (Bioline) in both biological and technical triplicate. Reactions were carried out and analyzed using a QuantStudio5 machine (Applied Biosystems). See Table S5 for qRT-PCR primer sequences.

CUT&RUN Library Preparation

CUT&RUN libraries were generated by first lysing 300,000-500,000 cells in 500μL of Nuclei Extraction Buffer (20mM HEPES-KOH pH 7.9, 10mM KCl, 1mM $MgCl_2$, 0.1% Triton X-100, 20% glycerol, and 1x protease inhibitor) for 10 minutes on ice.. Next, samples were spun down and washed twice with Nuclei Extraction Buffer before being resuspended in 500μL nuclei extraction buffer. 10μL of Concanavalin A-coated beads (EpiCypher) previously washed in Wash Buffer (20mM HEPES-KOH pH 7.5, 150mM NaCl, 2mM EDTA, 0.5mM spermidine, and 1x protease inhibitor) and resuspended in Binding Buffer (20mM HEPES-KOH pH 7.5, 1mM $CaCl_2$, and 1mM $MnCl_2$) were then added to the samples and incubated with rotation for 15 min at 4°C. Next, samples were washed once with Binding Buffer before being resuspended in 50 μL of Buffer 2 containing 0.1%BSA, 2μM EDTA and 0.5μL H3K27me3 1˚ antibody, followed by overnight incubation with rotation at 4°C. Following the incubation, samples were washed twice with Buffer 2 before being incubated in 50μL of Buffer 2 containing ~700ng/mL protein A-MNase fusion protein (Batch #6 from the Henikoff Lab) for 1 hour with rotation at 4°C. Samples were washed two more times and resuspended in 100 μL of Buffer 2 before starting the MNase digestion by adding $CaCl_2$ to a concentration of 2mM on ice for 30 minutes, after which the reaction was quenched with the addition of 100 μL 2X Stop Buffer (200mM NaCl, 20mM EDTA, 4mM EGTA, 50μg/mL RNase A, 40μg/mL GlycoBlue (Ambion), and 2pg/mL spike-in DNA) to inactivate the MNase. Samples were incubated for 30 min at 37°C and spun down for 5 minutes at 4°C to

release DNA fragments. DNA was phenol:chloroform extracted and 200μL of the recovered aqueous phase was ethanol precipitated with 500μL ethanol, 20μL 3M NaOAc, 2μL GlycoBlue at -80˚C. Libraries were prepared using 2S Plus DNA Library Kit adapters (Swift Biosciences) and size-selected using SPRIselect beads (Beckman Coulter) before being amplified and sent for paired-end sequencing on the NovaSeq 6000 (150 bp reads).

CUT&RUN Processing and Analysis

CUT&RUN paired reads were aligned to a reference human genome (hg38) by the bwa-mem algorithm. PCR duplicate reads were removed by Picardand peaks were called using macs2 with the broad flag and an FDR of 0.05. Bedtools intersect was used to identify reproducible peaks between biological replicates of each condition, and reproducible peaks from each condition were compiled into a list. Bedtools multicov was used to build a matrix with the number of reads from each dataset falling in each region in this list. This matrix was used for all 'genome wide' analyses. Bedtools multicov was also used to build a matrix with the number of reads from each dataset in a 5,000bp window around the transcription start site (4kb upstream, 1kb downstream) of all hg38 genes defined by gencode v41. The gencode v41annotation for CCND2 was originally incorrectly assigned to chr12:4,265,771-4,270,771 and reassigned using the Refseq coordinates chr12:4,269,762-4,274,762. Count matrices were analyzed with DESeq2 to compare changes in H3K27me3 deposition globally, and changes in H3K27me3 deposition in promoters. For heatmaps, deduplicated BAM files were converted to bigwigs and BED files and normalized reads per kilobase per million mapped read using deepTools bamCoverage. For genome wide analyses, H3K27me3 CUT&RUN signal in normalized bigwigs was measured using deepTools computeMatrix in 10kb regions centered around WT peaks overlapping with CpG islands. For promoter analyses, H3K27me3 CUT&RUN signal in normalized bigwigs was measured using deepTools computeMatrix in 5kb regions (4kb upstream, 1kb downstream) around transcription start sites for promoters overlapping with CpG islands. Promoters with the highest average H3K27me3 signal intensity in Wild-type replicate 1 and sorted in descending order.

RNA-Seq Processing and Analysis

RNA-seq paired reads were quantified using Salmon. Transcript-level abundance estimates from Salmon and gene-level count matrices were created using Tximport and analyzed using DESeq2. Paired reads were aligned using STAR to generate BAM files. BAM files were converted to BED files using bamCoverage and normalized using RPKMs and to effective genome size of hg38 (2,913,022,398) with a bin size of 10.

Figure Legends

Figure 1: Chemogenomics CRISPR-Cas9 Screen to Study Cell Cycle Progression

(A): Schematic of whole-genome CRISPR-Cas9 screen.

(B): Volcano plots and 1nM camptothecin whole-genome screen results. The Orobas calculated "Differential Gene Effect" was plotted against the -$\log_{10}$(p-value) for this effect for each gene targeted in the screen, as calculated by the Orobas pipeline. Red dotted line indicates the established cut-off. Highlighted dots are genes with known roles in response to each treatment, with blue or yellow dots indicate genes that when inactivated resulted in sensitivity or resistance, respectively, to camptothecin.

(C): Representative STRING analysis networks for protein complexes with known roles in pathways that we identified as sensitive in our 1nM camptothecin chemogenomics screen. Blue dots in the STRING network indicate genes that when inactivated resulted in sensitivity to camptothecin.

(D): Same as in (B) but for 9.2nM colchicine whole-genome screen results.

(E): Same as in (C) but for 9.2nM colchicine whole-genome screen results.

(F): Same as in (B) but for 0.7μM palbociclib whole-genome screen results.

(G): Same as in (C) but for 0.7μM palbociclib whole-genome screen results.

Figure 2: Analysis of Camptothecin and Colchicine Chemogenomics Screen Reveals Novel Players in Cell Cycle Regulation

(A): Dot plot comparison of the effect of gene mutation across three different screen conditions. Circle color indicates the strength of the positive or negative differential gene effect, circle size indicates its $-\log_{10}$(p-value) from our Orobas analysis.

(B): Volcano plot of novel genes identified in the 1nM camptothecin chemogenomics screen. Volcano plots are plotted as in (Fig. 1B), with highlighted dots representing novel genes identified in the camptothecin screen.

(C): Dot plot of Metascape analysis of significant genes that sensitized or de-sensitized cells to 1nM camptothecin. The $-\log_{10}$(p-value) was plotted against each term. The Metascape determined enrichment for observed over expected genes associated with a given term is indicated by color of circle. The percentage of the genes above our established cut-off associated with a given term is indicated by the size of the circle.

(D): STRING analysis of genes identified from our analysis of the 1nM camptothecin chemogenomics screen.

(E), (F) and (G) Same as in (B), (C) and (D) except for 9.2nM colchicine chemogenomics screen.

Figure 3: Mutation of Mitochondria Genes Attenuates the Sensitivity to Palbociclib

(A): Dot plot of Metascape analysis of significant genes in the 0.7μM palbociclib chemogenomics screen. The $-\log_{10}$(p-value) was plotted against each term. The Metascape determined enrichment for observed over expected genes associated with a given term is indicated by color of circle. The percentage of the genes above our established cut-off are associated with a given term is indicated by the size of the circle.

(B): Volcano plot of genes identified from our analysis of the 0.7μM palbociclib chemogenomics screen. Volcano plots are plotted as in Fig. 1D, with highlighted dots representing novel genes identified in the palbociclib screen.

(C): STRING networks of novel protein complexes identified in palbociclib screen. Dots in the STRING network indicate genes that when inactivated resulted in sensitivity (blue, left) of resistance (yellow, right) to 0.7μM palbociclib.

(D): Dose-response curve of palbociclib-induced growth inhibition with oxidative phosphorylation inhibitors. HAP1 cells were exposed to palbociclib with or without increasing concentrations of the oxidative phosphorylation inhibitors rotenone, TTFA and oligomycin. Cell proliferation in each treatment was determined after 48 hours by PrestoBlue assay. All data were normalized to the initial dose of each oxidative phosphorylation inhibitor in indicated concentration of palbociclib. Error bars represent the mean of three replicates ±StdDev.

Figure 4: Loss of Polycomb Repressive Complex Components Display Specific Resistance to Palbociclib

(A): Volcano plots in Fig. 3B except with members of PR-DUB, Polycomb Repressive Complex 1 and 2 highlighted.

(B): STRING analysis network of Polycomb Repressive Complex components. Yellow dots in STRING network indicate that inactivation of these genes conferred resistance to 0.7μM palbociclib in our chemogenomics screen.

(C): Dot plot of comparison of the effect of PRC2 complex member gene mutation across three different screen conditions, as in Fig. 2B.

(D): Dose-response curve of a nine-day quantitative Crystal Violet assay demonstrating rescue of palbociclib-induced growth inhibition with GSK126. All data were normalized to untreated cells and represents the mean of three technical replicates ±StdDev.

(E): Results of competitive growth assay for each indicated time point, normalized to the initial GFP+/GFP- ratio of the pool. The performance of each sgRNA in 1.5μM palbociclib vs Mock is shown, after normalizing to the control sgRNA. Data represents the mean ±SEM of the GFP+/GFP- ratios of three independent sgRNAs.

(F): Dose-response curve of nine-day quantitative Crystal Violet assay results demonstrating rescue of palbociclib-induced growth in MTF2Δ and JARID2Δ cells. Data represent mean Crystal Violet staining of cell culture wells of three independently isolated monoclonal knockout cell lines ±StdDev.

(G): BrdU incorporation assay for Wild-type, SUZ12Δ, MTF2Δ and JARID2Δ cell lines were incubated in 1.5μM palbociclib for 24 hours. *Left* – Representative BrdU incorporation vs propidium iodide FACS analysis. *Right* – Quantification of BrdU incorporation assay. Data represents the mean S-phase cells for three independently isolated monoclonal cell lines ±StDev. *: p-value<0.05, n.s.: not significant, as determined by two-tailed unpaired Student's t-test.

Figure 5: Polycomb 2.1 and PRC2.2 are Differentially Recruited to Promoters with CpG Island in HAP1
(A): *Left* - Western blot of Wild-type, SUZ12Δ, MTF2Δ and JARID2Δ HAP1 cell lines, probed with the indicated antibodies. *Right* –Quantification of H3K27me3 signal, normalized to H3 intensity. Each bar represents mean normalized H3K27me3 signal intensity across three independently isolated monoclonal cell lines ±StDev. *: p-value<0.05, n.s.: not significant, as determined by two-tailed unpaired Student's t-test.
(B): *Left* - Venn diagram of the overlap in promoters with decreased H3K27me3 read counts in CUT&RUN experiment between MTF2Δ or JARID2Δ cell lines compared to Wild-type cells. Promoters with differential enrichment of H3K27me3 total counts for a promoter was considered significant if the between monoclonal knockout and Wild-type $\log_2$ fold-change was ±1 and the adjusted p-value <0.1. *Right* - Venn diagram of the overlap in differentially increased transcript levels in RNA-Seq experiment between MTF2Δ or JARID2Δ cell lines compared to Wild-type cells. A transcript was considered as significantly differentially expressed if the $\log_2$ fold-change was ±1 and the adjusted p-value <0.05.
(C): Dot-plot of selected Metascape terms from analysis of promoters or mRNAs annotated as protein coding genes and displaying either significantly increased or decreased levels of H3K27me3 or transcripts. Color of the circle indicates the $-\log_{10}$(p-value) of the term and the size of circle indicates the percentage of the genes from the input list were represented in that term.
(D): Bedgraphs of promoters with significantly decreased H3K27me3 and increased transcripts that was either specifically dependent on MTF2 (*left*), JARID2 (*center*) or co-dependent on the presence either MTF2 or JARID2 (*right*). Tracks represent combined BED files from two clonal biological replicates.
(E): Heat map of H3K27me3 signal over a 10kb window for 1,877 peaks overlapping with CpG islands with the highest average signal intensity were identified in wild-type cells and plotted for the same loci in MTF2Δ and JARID2Δ cells. Plots are of one replicate of the two biological replicates used in the CUT&RUN experiment. CGI: CpG Island.
(F): *Left* – Heat map of H3K27me3 signal in promoters containing at least one CpG island for the top 2,000 promoters with the highest average H3K27me3 signal were identified in wild-type cells and plotted for the same loci in MTF2Δ and JARID2Δ cells in 5kb window around transcription start site (TSS). Left boarder of plot is -4kb from TSS, right boarder is +1kb from TSS. Plots are of one replicate of the two biological replicates used in the CUT&RUN experiment. *Right* - CUT&RUN signal averaged for all 25,124 CpG island-containing promoters for wild-type, MTF2Δ, and JARID2Δ cells in 5kb window around transcription start site (TSS).
(G): Bar plot of $\log_{10}$(p-value) of Reactome (teal bars) and MSigDB (red bars) terms associated with protein coding genes that contain at least one CpG island.

Figure 6: CCND1 and CCND2 Expression is Increased in MTF2Δ Mutants
(A): Volcano plot of DESeq2 calculated changes in $\log_2$ fold-change in H3K27me3 signal in promoters versus the $\log_{10}$(p-value) in enrichment in MTF2Δ cells determined by CUT&RUN.
(B): Same as in (A) but for transcript abundance determined by RNA-seq.
(C): Scatterplot of $\log_2$ fold-changes calculated by DESeq2 for MTF2Δ/Wild-type ratio of mRNA expression in the RNA-seq (x-axis) versus H3K27me3 signal in promoters from our CUT&RUN (y-axis) experiments. Genes whose $\log_2$ fold change in the RNA-seq experiment had an adjusted p-value of <0.05 and an adjusted p-value <0.1 in the CUT&RUN experiment where plotted.
(D): Bedgraph of H3K27me3 and transcript signal as well as CpG island location within the CCND1 promoter region (chr11:69,634,655-69,644,656; CpG island coordinates - chr11:69,636,368-69,643,828) and CCND2 promoter region (chr12:4,266,723-4,280,248; CpG island coordinates - chr12:4,269,237-4,275,239).

(E): *Top* – Western blots of Cas9-expressing pools of HAP1 cells transduced three independent sgRNAs targeting the indicated genes. Membranes were probed with the indicated antibodies *Bottom* – Quantification of CCND1, CCND2 and CCND3 signal, normalized to ß-actin intensity in HAP1 pooled knockouts. Mean signal intensity for three independent sgRNAs was plotted ±StDev. *: p-value<0.05, **: p-value<0.005, ***: p-value<0.0005, n.s.: not significant, Two tailed unpaired Student's t-test.
(F): qRT-PCR relative quantification of CCND1, CCND2 and CCND3 mRNA levels in monoclonal wild-type, SUZ12Δ, MTF2Δ and JARID2Δ cells. Each bar is the mean for three biological replicates, each in performed in technical triplicate, ±StDev. *: p-value<0.05, **: p-value<0.005, ***: p-value<0.0005, n.s.: not significant, two tailed unpaired Student's t-test.
(G): Same as in (E), but in wild-type, SUZ12Δ, MTF2Δ and JARID2Δ monoclonal cell lines. The same protein extracts used in Fig. 5A were used here, but membranes probed with indicated antibodies.
(H): *Left* – Representative Western blot of total RB1 and P-S807/8111-RB1 with increasing [palbociclib] in WT, MTF2Δ and JARID2Δ cells. Membranes were probed with secondary antibodies against mouse (RB1) or rabbit (P-S807/8111-RB1) conjugated to different fluorophores to enable simultaneous detection of phosphorylated and total forms of RB1. *Right* – Quantification of the ratio of P-S807/8111-RB1 to total RB1 signal determined by Western blot, plotted against [palbociclib]. Each point represents the P-RB1/RB1 ratio for two independently isolated monoclonal cell lines, error bars ±range. The experiment was repeated three times with similar results.

Supplemental Figure Legends

Supplementary Figure 1: Dosing to Determine Inhibitor Concentration for Chemogenomics Screen
(S1A): Drug dosing experiments were performed to determine screening concentrations. Cells were counted during passage in increasing doses of camptothecin (*left*), palbociclib (*center*) and colchicine (*right*).
(S1B): Representative images of flow cytometry traces from untreated cells or cells treated with 0.7μM palbociclib, 9.2nM colchicine or 1nM camptothecin treated cells for three days, then stained propidium iodide. Plots represent the number of stained cells with a given propidium iodide intensity.
(S1C): Venn diagrams showing overlap for significant genes that sensitized (*left*) or de-sensitized cells (*right*) to each condition tested. Genes that were determined as significant in all three screens were omitted in further analyses (see Table S2 for a list of the omitted genes).

Supplementary Figure 2: Assays to Determine Resistance of PRC2 Component Mutants to CDK4/6 Inhibitors
(S2A): Schematic of internally controlled competitive growth assay used to validate chemogenomics results or monoclonal cell line proliferation when treated with palbociclib. In experiments where we generated polyclonal pooled knockouts, GFP^+ cells expressing Cas9 were mixed with GFP^- cells without Cas9 (as in Fig 4E). For competitive growth experiments with monoclonal knockout cell lines, GFP^+, Cas9 expressing cells were mixed with GFP^- monoclonal knockout lines (as in Fig. S2C).
(S2B): Western blots demonstrating the efficacy of indicated sgRNA used in our competitive growth assay and use of polyclonal pooled knockouts. Cells were transduced with the indicated sgRNA, Cas9 expression was then induced for three days with doxycycline to generate polyclonal pooled knockouts. Whole-cell lysates from these pooled knockouts were then probed with antibodies against the indicated proteins.
(S2C): Competitive growth assay for or monoclonal knockout cell lines. Wild-type, MTF2Δ and JARID2Δ cell lines (GFP^-) were mixed with wild-type HAP1 cells expressing Cas9 and GFP (GFP^+) and treated with either DMSO (mock) or 1.5μM palbociclib (*left*), 3.5μM ribociclib (*center*) or 0.4μM abemaciclib (*right*) for twelve days. Cells were split every three days and the GFP^-/GFP^+ ratio was assessed every six days by flow cytometry.
(S2D): Western blot of protein extracts from cells treated with DMSO (mock) or 1.5μM palbociclib for 48 hours, probed with indicated antibody. PARP cleavage and BIM over expression controls are included in the

last lane from protein extracts from RPE1 cells over-expressing a doxycycline-inducible HA-tagged BIM to induce apoptosis.

Supplementary Figure 3: Analysis of Changes in H3K27me3 Distribution in CUT&RUN and Differentially Expressed Genes in RNA-Seq Experiments

(S3A): *Top* - PCA plot of H3K27me3 peaks called by macs2 from CUT&RUN experiment done in biological duplicate. *Bottom* – PCA plot of RNA-seq reads for experiment done in biological triplicate.

(S3B): Venn diagrams of the Gencode Annotations of promoters that had significantly up regulated (top row) and down regulated H3K27me3 (bottom row) from our CUT&RUN experiment for MTF2Δ (*left*) and JARID2Δ cells (*right*). Significant promoters were determined as having a $\log_2$ fold change ±1 and an adjusted p-value of <0.1.

(S3C): Same as in (S3B) only for our RNA-Seq experiments and significant promoters were determined as having a $\log_2$ fold change ±1 and an adjusted p-value < 0.05.

(S3D): Average H3K27me3 distribution over a 10kb window for 1,877 peaks overlapping with CpG islands with the highest average signal intensity were identified in Wild-type cells and plotted for the same loci in MTF2Δ and JARID2Δ cells.

(S3E): Bar plot of $-\log_{10}$(p-value) for the enrichment of a given transcription factors from ENCODE and ChEA databases binding to the list of promoters with overlapping CpG islands and H3K27me3 peaks.

Supplementary Figure 4: Analysis of Differential H3K27me3 Distribution and Transcript Expression of D-type Cyclins in CUT&RUN and RNA-Seq Data Sets

(S4A): Volcano plot of DESeq2 calculated changes in $\log_2$ fold-change in H3K27me3 signal in promoters versus the $\log_{10}$(p-value) in enrichment in JARID2Δ cells determined by CUT&RUN. CCND1 and CCND2 location within the dataset are indicated by yellow dots.

(S4B): Same as in (A) but for transcript abundance determined by RNA-seq.

(S4C): Scatter plot of $\log_2$ fold-change in transcript abundance vs H3K27me3 promoter signal for genes with an adjusted p-value <0.1 in our CUT&RUN and adjusted p-value <0.05 in our RNA-Seq from our JARID2Δ cell lines.

(S4D): Bedgraph of H3K27me3, transcript coverage and CpG island location within the CCND3 promoter region (chr6:41,940,179-4,195,017; CpG island coordinates: chr6:41,941,008-41,941,973).

(S4E): Quantification of protein signal from Western blot in Fig. 6G for CCND1 (*left*), CCND2 (*center*), and CCND3 (*right*) normalized to Actin. Each bar is the mean for three biological replicates, error bars ±StDev. *: p-value<0.05, **: p-value<0.005, ***: p-value<0.0005, n.s.: not significant, two tailed unpaired Student's t-test.

(S4F): Dot plot of $\log_2$ fold-change for indicated mRNAs in MTF2Δ and JARID2Δ cells as determined by DESeq2. Established cut of ±1 $\log_2$ fold-change in transcript abundance indicated by dashed grey line.

(S4G): Western blot for a panel of G1 regulators from whole-cell lysates of wild-type, SUZ12Δ, MTF2Δ and JARID2Δ cell lines from three independently isolated monoclonal knockouts. Membranes were probed with the indicated antibodies.

References

1. Ginzberg MB, Kafri R, Kirschner M. On being the right (cell) size. Science (80-). 2015;348(6236). doi:10.1126/science.1245075
2. Massagué J. G1 cell-cycle control and cancer. Nature. 2004;432(7015):298-306. doi:10.1038/nature03094
3. Bertoli C, Skotheim JM, De Bruin RAM. Control of cell cycle transcription during G1 and S phases. Nat Rev Mol Cell Biol. 2013;14(8):518-528. doi:10.1038/nrm3629
4. Rubin SM, Sage J, Skotheim JM. Integrating Old and New Paradigms of G1/S Control. Mol Cell.

2020;80(2):183-192. doi:10.1016/j.molcel.2020.08.020
5. Malumbres M, Barbacid M. Mammalian cyclin-dependent kinases. Trends Biochem Sci. 2005;30(11):630-641. doi:10.1016/j.tibs.2005.09.005
6. Bracken AP, Ciro M, Cocito A, Helin K. E2F target genes: Unraveling the biology. Trends Biochem Sci. 2004;29(8):409-417. doi:10.1016/j.tibs.2004.06.006
7. Dickler MN, Tolaney SM, Rugo HS, et al. MONARCH 1, a phase II study of abemaciclib, a CDK4 and CDK6 inhibitor, as a single agent, n patients with refractory HR+/HER2- metastatic breast cancer. Clin Cancer Res. 2017;23(17):5218-5224. doi:10.1158/1078-0432.CCR-17-0754
8. Morrison L, Loibl S, Turner NC. The CDK4/6 inhibitor revolution — a game-changing era for breast cancer treatment. Nat Rev Clin Oncol. 2023. doi:10.1038/s41571-023-00840-4
9. Turner NC, Slamon DJ, Ro J, et al. Overall Survival with Palbociclib and Fulvestrant in Advanced Breast Cancer. N Engl J Med. 2018;379(20):1926-1936. doi:10.1056/nejmoa1810527
10. Im S-A, Lu Y-S, Bardia A, et al. Overall Survival with Ribociclib plus Endocrine Therapy in Breast Cancer. N Engl J Med. 2019;381(4):307-316. doi:10.1056/nejmoa1903765
11. Goel S, Bergholz JS, Zhao JJ. Targeting CDK4 and CDK6 in cancer. Nat Rev Cancer. 2022;22(6):356-372. doi:10.1038/s41568-022-00456-3
12. Cappell SD, Mark KG, Garbett D, Pack LR, Rape M, Meyer T. EMI1 switches from being a substrate to an inhibitor of APC/CCDH1 to start the cell cycle. Nature. 2018;558(7709):313-317. doi:10.1038/s41586-018-0199-7
13. Cappell SD, Chung M, Jaimovich A, Spencer SL, Meyer T. Irreversible APCCdh1 Inactivation Underlies the Point of No Return for Cell-Cycle Entry. Cell. 2016;166(1):167-180. doi:10.1016/j.cell.2016.05.077
14. Chung M, Liu C, Yang HW, Köberlin MS, Cappell SD, Meyer T. Transient Hysteresis in CDK4/6 Activity Underlies Passage of the Restriction Point in G1. Mol Cell. 2019;76(4):562-573.e4. doi:10.1016/j.molcel.2019.08.020
15. Zatulovskiy E, Zhang S, Berenson DF, Topacio BR, Skotheim JM. Cell growth dilutes the cell cycle inhibitor Rb to trigger cell division. Science (80-). 2020;369(6502):466-471. doi:10.1126/science.aaz6213
16. Lewis EB. A gene complex controlling segmentation in Drosophila. Nature. 1978;276(5688):565-570. doi:10.1038/276565a0
17. Dumesic PA, Homer CM, Moresco JJ, et al. Product binding enforces the genomic specificity of a yeast Polycomb repressive complex. Cell. 2015;160(1-2):204-218. doi:10.1016/j.cell.2014.11.039
18. Grimaud C, Bantignies F, Pal-Bhadra M, Ghana P, Bhadra U, Cavalli G. RNAi components are required for nuclear clustering of polycomb group response elements. Cell. 2006;124(5):957-971. doi:10.1016/j.cell.2006.01.036
19. Jamieson K, Rountree MR, Lewis ZA, Stajich JE, Selker EU. Regional control of histone H3 lysine 27 methylation in Neurospora. Proc Natl Acad Sci U S A. 2013;110(15):6027-6032. doi:10.1073/pnas.1303750110
20. Schuettengruber B, Bourbon HM, Di Croce L, Cavalli G. Genome Regulation by Polycomb and Trithorax: 70 Years and Counting. Cell. 2017;171(1):34-57. doi:10.1016/j.cell.2017.08.002
21. Kuroda MI, Kang H, De S, Kassis JA. Dynamic Competition of Polycomb and Trithorax in Transcriptional Programming. Annu Rev Biochem. 2020;89:235-253. doi:10.1146/annurev-biochem-120219-103641
22. Son J, Shen SS, Margueron R, Reinberg D. Nucleosome-binding activities within JARID2 and EZH1 regulate the function of PRC2 on chromatin. Genes Dev. 2013;27(24):2663-2677. doi:10.1101/gad.225888.113
23. Hauri S, Comoglio F, Seimiya M, et al. A High-Density Map for Navigating the Human Polycomb Complexome. Cell Rep. 2016;17(2):583-595. doi:10.1016/j.celrep.2016.08.096
24. van Mierlo G, Veenstra GJC, Vermeulen M, Marks H. The Complexity of PRC2 Subcomplexes. Trends

Cell Biol. 2019;29(8):660-671. doi:10.1016/j.tcb.2019.05.004
25. Piunti A, Shilatifard A. The roles of Polycomb repressive complexes in mammalian development and cancer. Nat Rev Mol Cell Biol. 2021;22(5):326-345. doi:10.1038/s41580-021-00341-1
26. Lesley Brown J, Sun M an, Kassis JA. Global changes of H3K27me3 domains and Polycomb group protein distribution in the absence of recruiters Spps or Pho. Proc Natl Acad Sci U S A. 2018;115(8):E1839-E1848. doi:10.1073/pnas.1716299115
27. De S, Gehred ND, Fujioka M, Chan FW, Jaynes JB, Kassis JA. Defining the boundaries of polycomb domains in drosophila. Genetics. 2020;216(3):689-700. doi:10.1534/genetics.120.303642
28. Li H, Liefke R, Jiang J, et al. Polycomb-like proteins link the PRC2 complex to CpG islands. Nature. 2017;549(7671):287-291. doi:10.1038/nature23881
29. Perino M, Van Mierlo G, Karemaker ID, et al. MTF2 recruits Polycomb Repressive Complex 2 by helical-shape-selective DNA binding. Nat Genet. 2018;50(7):1002-1010. doi:10.1038/s41588-018-0134-8
30. Barbour H, Daou S, Hendzel M, Affar EB. Polycomb group-mediated histone H2A monoubiquitination in epigenome regulation and nuclear processes. Nat Commun. 2020;11(1):1-16. doi:10.1038/s41467-020-19722-9
31. Cooper S, Grijzenhout A, Underwood E, et al. Jarid2 binds mono-ubiquitylated H2A lysine 119 to mediate crosstalk between Polycomb complexes PRC1 and PRC2. Nat Commun. 2016;7:1-8. doi:10.1038/ncomms13661
32. Kalb R, Latwiel S, Baymaz HI, et al. Histone H2A monoubiquitination promotes histone H3 methylation in Polycomb repression. Nat Struct Mol Biol. 2014;21(6):569-571. doi:10.1038/nsmb.2833
33. Glancy E, Wang C, Tuck E, et al. PRC2.1- and PRC2.2-specific accessory proteins drive recruitment of different forms of canonical PRC1. Mol Cell. 2023;83(9):1393-1411.e7. doi:10.1016/j.molcel.2023.03.018
34. Kasinath V, Beck C, Sauer P, et al. JARID2 and AEBP2 regulate PRC2 in the presence of H2AK119ub1 and other histone modifications. Science (80-). 2021;371(6527). doi:10.1126/science.abc3393
35. Chen S, Jiao L, Shubbar M, Yang X, Liu X. Unique Structural Platforms of Suz12 Dictate Distinct Classes of PRC2 for Chromatin Binding. Mol Cell. 2018;69(5):840-852.e5. doi:10.1016/j.molcel.2018.01.039
36. Su CL, Deng TR, Shang Z, Xiao Y. JARID2 inhibits leukemia cell proliferation by regulating CCND1 expression. Int J Hematol. 2015;102(1):76-85. doi:10.1007/s12185-015-1797-x
37. Shirato H, Ogawa S, Nakajima K, et al. A jumonji (Jarid2) protein complex represses cyclin D1 expression by methylation of histone H3-K9. J Biol Chem. 2009;284(2):733-739. doi:10.1074/jbc.M804994200
38. Adhikari A, Davie J. JARID2 and the PRC2 complex regulate skeletal muscle differentiation through regulation of canonical Wnt signaling. Epigenetics and Chromatin. 2018;11(1):1-20. doi:10.1186/s13072-018-0217-x
39. Petracovici A, Bonasio R. Distinct PRC2 subunits regulate maintenance and establishment of Polycomb repression during differentiation. Mol Cell. 2021;81(12):2625-2639.e5. doi:10.1016/j.molcel.2021.03.038
40. Loh CH, van Genesen S, Perino M, Bark MR, Veenstra GJC. Loss of PRC2 subunits primes lineage choice during exit of pluripotency. Nat Commun. 2021;12(1):1-14. doi:10.1038/s41467-021-27314-4
41. Rothberg JLM, Maganti HB, Jrade H, et al. Mtf2-PRC2 control of canonical Wnt signaling is required for definitive erythropoiesis. Cell Discov. 2018;4(1). doi:10.1038/s41421-018-0022-5
42. Ngubo M, Moradi F, Ito, Caryn Y. Stanford WL. Tissue-Specific Tumour Suppressor and Oncogenic Activities of the Polycomb-like Protein MTF2. 2023.
43. Bracken AP, Kleine-Kohlbrecher D, Dietrich N, et al. The Polycomb group proteins bind throughout the INK4A-ARF locus and are disassociated in senescent cells. Genes Dev. 2007;37(17-18):861. doi:10.1101/gad.351178.123

44. Bracken AP, Pasini D, Capra M, Prosperini E, Colli E, Helin K. EZH2 is downstream of the pRB-E2F pathway, essential for proliferation and amplified in cancer. EMBO J. 2003;22(20):5323-5335. doi:10.1093/emboj/cdg542
45. Bracken AP, Dietrich N, Pasini D, Hansen KH, Helin K. Genome-wide mapping of polycomb target genes unravels their roles in cell fate transitions. Genes Dev. 2006;20(9):1123-1136. doi:10.1101/gad.381706
46. Adhikari A, Mainali P, Davie JK. JARID2 and the PRC2 complex regulate the cell cycle in skeletal muscle. J Biol Chem. 2019;294(51):19451-19464. doi:10.1074/jbc.RA119.010060
47. Adhikari A, Davie JK. The PRC2 complex directly regulates the cell cycle and controls proliferation in skeletal muscle. Cell Cycle. 2020;19(18):2373-2394. doi:10.1080/15384101.2020.1806448
48. Horlbeck MA, Xu A, Wang M, et al. Mapping the Genetic Landscape of Human Cells. Cell. 2018;174(4):953-967.e22. doi:10.1016/j.cell.2018.06.010
49. Przybyla L, Gilbert LA. A new era in functional genomics screens. Nat Rev Genet. 2022;23(2):89-103. doi:10.1038/s41576-021-00409-w
50. Bock C, Datlinger P, Chardon F, et al. High-content CRISPR screening. Nat Rev Methods Prim. 2022;2(1). doi:10.1038/s43586-021-00093-4
51. Hundley F V., Sanvisens Delgado N, Marin HC, Carr KL, Tian R, Toczyski DP. A comprehensive phenotypic CRISPR-Cas9 screen of the ubiquitin pathway uncovers roles of ubiquitin ligases in mitosis. Mol Cell. 2021;81(6):1319-1336.e9. doi:10.1016/j.molcel.2021.01.014
52. Stok C, Tsaridou S, van den Tempel N, et al. FIRRM/C1orf112 is synthetic lethal with PICH and mediates RAD51 dynamics. Cell Rep. 2023;42(7). doi:10.1016/j.celrep.2023.112668
53. Aregger M, Lawson KA, Billmann M, et al. Systematic mapping of genetic interactions for de novo fatty acid synthesis identifies C12orf49 as a regulator of lipid metabolism. Nat Metab. 2020;2(6):499-513. doi:10.1038/s42255-020-0211-z.Systematic
54. Hundley F V., Toczyski DP. Chemical-genetic CRISPR-Cas9 screens in human cells using a pathway-specific library. STAR Protoc. 2021;2(3):100685. doi:10.1016/j.xpro.2021.100685
55. Olbrich T, Vega-Sendino M, Murga M, et al. A Chemical Screen Identifies Compounds Capable of Selecting for Haploidy in Mammalian Cells. Cell Rep. 2019;28(3):597-604.e4. doi:10.1016/j.celrep.2019.06.060
56. Llargués-Sistac G, Bonjoch L, Castellvi-Bel S. HAP1, a new revolutionary cell model for gene editing using CRISPR-Cas9. Front Cell Dev Biol. 2023;11(March):1-10. doi:10.3389/fcell.2023.1111488
57. Hart T, Tong AHY, Chan K, et al. Evaluation and design of genome-wide CRISPR/SpCas9 knockout screens. G3 Genes, Genomes, Genet. 2017;7(8):2719-2727. doi:10.1534/g3.117.041277
58. Su D, Feng X, Colic M, et al. CRISPR/CAS9-based DNA damage response screens reveal gene-drug interactions. DNA Repair (Amst). 2020;87(November 2019):102803. doi:10.1016/j.dnarep.2020.102803
59. Groelly FJ, Fawkes M, Dagg RA, Blackford AN, Tarsounas M. Targeting DNA damage response pathways in cancer. Nat Rev Cancer. 2023;23(2):78-94. doi:10.1038/s41568-022-00535-5
60. Hsiang YH, Hertzberg R, Hecht S, Liu LF. Camptothecin induces protein-linked DNA breaks via mammalian DNA topoisomerase I. J Biol Chem. 1985;260(27):14873-14878. doi:10.1016/s0021-9258(17)38654-4
61. Dalbeth N, Lauterio TJ, Wolfe HR. Mechanism of action of colchicine in the treatment of gout. Clin Ther. 2014;36(10):1465-1479. doi:10.1016/j.clinthera.2014.07.017
62. Xie X, Hu H, Tong X, et al. The mTOR-S6K Pathway Links Growth Signaling to DNA Damage Response by Targeting RNF168. Nat Cell Biol. 2018;20(3):320-331. doi:10.1038/s41556-017-0033-8.The
63. Bader AS, Hawley BR, Wilczynska A, Bushell M. The roles of RNA in DNA double-strand break repair. Br J Cancer. 2020;122(5):613-623. doi:10.1038/s41416-019-0624-1
64. Stadler J, Richly H. Regulation of DNA repair mechanisms: How the chromatin environment regulates

the DNA damage response. Int J Mol Sci. 2017;18(8). doi:10.3390/ijms18081715
65. Crozier L, Foy R, Adib R, et al. CDK4/6 inhibitor-mediated cell overgrowth triggers osmotic and replication stress to promote senescence. Mol Cell. 2023;83(22):4062-4077.e5. doi:10.1016/j.molcel.2023.10.016
66. Crozier L, Foy R, Mouery BL, et al. CDK4/6 inhibitors induce replication stress to cause long-term cell cycle withdrawal. EMBO J. 2022;41(6):1-20. doi:10.15252/embj.2021108599
67. Rahman M, Billmann M, Costanzo M, et al. A method for benchmarking genetic screens reveals a predominant mitochondrial bias. Mol Syst Biol. 2021;17(5):1-12. doi:10.15252/msb.202010013
68. De La Fuente R. Histone deacetylation: Establishing a meiotic histone code. Cell Cycle. 2014;13(6):879-880. doi:10.4161/cc.28214
69. Chittock EC, Latwiel S, Miller TCR, Müller CW. Molecular architecture of polycomb repressive complexes. Biochem Soc Trans. 2017;45(1):193-205. doi:10.1042/BST20160173
70. Ismail IH, Davidson R, Gagné JP, Xu ZZ, Poirier GG, Hendzel MJ. Germline mutations in BAP1 impair its function in DNA double-strand break repair. Cancer Res. 2014;74(16):4282-4294. doi:10.1158/0008-5472.CAN-13-3109
71. Healy E, Mucha M, Glancy E, et al. PRC2.1 and PRC2.2 Synergize to Coordinate H3K27 Trimethylation. Mol Cell. 2019;76(3):437-452.e6. doi:10.1016/j.molcel.2019.08.012
72. Zhu Y, Dong L, Wang C, et al. Functional redundancy among Polycomb complexes in maintaining the pluripotent state of embryonic stem cells. Stem Cell Reports. 2022;17(5):1198-1214. doi:10.1016/j.stemcr.2022.02.020
73. Youmans DT, Gooding AR, Dowell RD, Cech TR. Competition between PRC2.1 and 2.2 subcomplexes regulates PRC2 chromatin occupancy in human stem cells. Mol Cell. 2021;81(3):488-501.e9. doi:10.1016/j.molcel.2020.11.044
74. Oliviero G, Brien GL, Waston A, et al. Dynamic protein interactions of the polycomb repressive complex 2 during differentiation of pluripotent cells. Mol Cell Proteomics. 2016;15(11):3450-3460. doi:10.1074/mcp.M116.062240
75. Smits AH, Jansen PWTC, Poser I, Hyman AA, Vermeulen M. Stoichiometry of chromatin-associated protein complexes revealed by label-free quantitative mass spectrometry-based proteomics. Nucleic Acids Res. 2013;41(1):1-8. doi:10.1093/nar/gks941
76. Jadhav U, Manieri E, Nalapareddy K, et al. Replicational Dilution of H3K27me3 in Mammalian Cells and the Role of Poised Promoters. Mol Cell. 2020;78(1):141-151.e5. doi:10.1016/j.molcel.2020.01.017
77. Zhu Z, Turner NC, Loi S, et al. Comparative biomarker analysis of PALOMA-2/3 trials for palbociclib. npj Precis Oncol. 2022;6(1). doi:10.1038/s41698-022-00297-1
78. Schoninger SF, Blain SW. The ongoing search for biomarkers of CDK4/6 inhibitor responsiveness in breast cancer. Mol Cancer Ther. 2020;19(1):3-12. doi:10.1158/1535-7163.MCT-19-0253
79. Dean JL, Thangavel C, McClendon AK, Reed CA, Knudsen ES. Therapeutic CDK4/6 inhibition in breast cancer: Key mechanisms of response and failure. Oncogene. 2010;29(28):4018-4032. doi:10.1038/onc.2010.154
80. Wang TH, Chen CC, Leu YL, et al. Palbociclib induces DNA damage and inhibits DNA repair to induce cellular senescence and apoptosis in oral squamous cell carcinoma. J Formos Med Assoc. 2021;120(9):1695-1705. doi:10.1016/j.jfma.2020.12.009
81. Sionov RV, Vlahopoulos SA, Granot Z. Regulation of Bim in health and disease. Oncotarget. 2015;6(27):23058-23134. doi:10.18632/oncotarget.5492
82. Watt AC, Cejas P, Decristo MJ, et al. CDK4/6 inhibition reprograms the breast cancer enhancer landscape by stimulating AP-1 transcriptional activity. Nat Cancer. 2021;2(1):34-48. doi:10.1038/s43018-020-00135-y.CDK4/6
83. Pancholi S, Ribas R, Simigdala N, et al. Tumour kinome re-wiring governs resistance to palbociclib in oestrogen receptor positive breast cancers, highlighting new therapeutic modalities. Oncogene. 2020;39(25):4781-4797. doi:10.1038/s41388-020-1284-6

84. Guarducci C, Bonechi M, Benelli M, et al. Cyclin E1 and Rb modulation as common events at time of resistance to palbociclib in hormone receptor-positive breast cancer. npj Breast Cancer. 2018;4(1):1-10. doi:10.1038/s41523-018-0092-4
85. Turner NC, Liu Y, Zhu Z, et al. Cyclin E1 expression and palbociclib efficacy in previously treated hormone receptor-positive metastatic breast cancer. J Clin Oncol. 2019;37(14):1169-1178. doi:10.1200/JCO.18.00925
86. Ferguson KM, Gillen SL, Chaytor L, et al. Palbociclib releases the latent differentiation capacity of neuroblastoma cells. Dev Cell. 2023;58(19):1967-1982.e8. doi:10.1016/j.devcel.2023.08.028
87. Lanceta L, Lypova N, O'Neill C, et al. Differential gene expression analysis of palbociclib-resistant TNBC via RNA-seq. Breast Cancer Res Treat. 2021;186(3):677-686. doi:10.1007/s10549-021-06127-5
88. German B, Ellis L. Polycomb Directed Cell Fate Decisions in Development and Cancer. Epigenomes. 2022;6(3):1-30. doi:10.3390/epigenomes6030028
89. Uzhachenko R V., Bharti V, Ouyang Z, et al. Metabolic modulation by CDK4/6 inhibitor promotes chemokine-mediated recruitment of T cells into mammary tumors. Cell Rep. 2021;35(1):108944. doi:10.1016/j.celrep.2021.108944
90. Franco J, Balaji U, Freinkman E, Witkiewicz AK, Knudsen ES. Metabolic Reprogramming of Pancreatic Cancer Mediated by CDK4/6 Inhibition Elicits Unique Vulnerabilities. Cell Rep. 2016;14(5):979-990. doi:10.1016/j.celrep.2015.12.094
91. Zheng Y, Huang G, Silva TC, et al. A pan-cancer analysis of CpG Island gene regulation reveals extensive plasticity within Polycomb target genes. Nat Commun. 2021;12(1):1-16. doi:10.1038/s41467-021-22720-0
92. Giangrande PH, Zhu W, Schlisio S, et al. A role for E2F6 in distinguishing G1/S- and G2/M-specific transcription. Genes Dev. 2004;18(23):2941-2951. doi:10.1101/gad.1239304
93. Shirahama Y, Yamamoto K. The e2f6 transcription factor is associated with the mammalian suz12-containing polycomb complex. Kurume Med J. 2020;67(4):171-183. doi:10.2739/kurumemedj.MS674006
94. Gong X, Litchfield LM, Webster Y, et al. Genomic Aberrations that Activate D-type Cyclins Are Associated with Enhanced Sensitivity to the CDK4 and CDK6 Inhibitor Abemaciclib. Cancer Cell. 2017;32(6):761-776.e6. doi:10.1016/j.ccell.2017.11.006
95. McCartney A, Migliaccio I, Bonechi M, et al. Mechanisms of Resistance to CDK4/6 Inhibitors: Potential Implications and Biomarkers for Clinical Practice. Front Oncol. 2019;9(July):2-9. doi:10.3389/fonc.2019.00666
96. Klein ME, Kovatcheva M, Davis LE, Tap WD, Koff A. CDK4/6 Inhibitors: The Mechanism of Action May Not Be as Simple as Once Thought. Cancer Cell. 2018;34(1):9-20. doi:10.1016/j.ccell.2018.03.023
97. Handschick K, Beuerlein K, Jurida L, et al. Cyclin-Dependent Kinase 6 Is a Chromatin-Bound Cofactor for NF-κB-Dependent Gene Expression. Mol Cell. 2014;53(2):193-208. doi:10.1016/j.molcel.2013.12.002
98. Otto T, Sicinski P. The kinase-independent, second life of CDK6 in transcription. Cancer Cell. 2013;24(2):141-143. doi:10.1016/j.ccr.2013.07.019
99. Santiappillai NT, Abuhammad S, Slater A, et al. CDK4/6 Inhibition Reprograms Mitochondrial Metabolism in BRAFV600 Melanoma via a p53 Dependent Pathway. Cancers (Basel). 2021;13(524):1-18.
100. Deng Q, Hou J, Feng L, et al. PHF19 promotes the proliferation, migration, and chemosensitivity of glioblastoma to doxorubicin through modulation of the SIAH1/β–catenin axis. Cell Death Dis. 2018;9(11). doi:10.1038/s41419-018-1082-z
101. Parreno V, Martinez AM, Cavalli G. Mechanisms of Polycomb group protein function in cancer. Cell Res. 2022;32(3):231-253. doi:10.1038/s41422-021-00606-6
102. Maganti HB, Jrade H, Cafariello C, et al. Targeting the MTF2–MDM2 axis sensitizes refractory acute

myeloid leukemia to chemotherapy. Cancer Discov. 2018;8(11):1376-1389. doi:10.1158/2159-8290.CD-17-0841
103. Liang Y, Yang Y, Guo R, et al. PCL2 regulates p53 stability and functions as a tumor suppressor in breast cancer. Sci Bull. 2018;63(10):629-639. doi:10.1016/j.scib.2018.03.012
104. Højfeldt JW, Hedehus L, Laugesen A, Tatar T, Wiehle L, Helin K. Non-core Subunits of the PRC2 Complex Are Collectively Required for Its Target-Site Specificity. Mol Cell. 2019;76(3):423-436.e3. doi:10.1016/j.molcel.2019.07.031
105. Walker E, Chang WY, Hunkapiller J, et al. Polycomb-like 2 Associates with PRC2 and Regulates Transcriptional Networks during Mouse Embryonic Stem Cell Self-Renewal and Differentiation. Cell Stem Cell. 2010;6(2):153-166. doi:10.1016/j.stem.2009.12.014
106. Landeira D, Sauer S, Poot R, et al. Jarid2 is a PRC2 component in embryonic stem cells required for multi-lineage differentiation and recruitment of PRC1 and RNA Polymerase II to developmental regulators. Nat Cell Biol. 2010;12(6):618-624. doi:10.1038/ncb2065
107. Pasini D, Cloos PAC, Walfridsson J, et al. JARID2 regulates binding of the Polycomb repressive complex 2 to target genes in ES cells. Nature. 2010;464(7286):306-310. doi:10.1038/nature08788
108. Kloet SL, Makowski MM, Baymaz HI, et al. The dynamic interactome and genomic targets of Polycomb complexes during stem-cell differentiation. Nat Struct Mol Biol. 2016;23(7):682-690. doi:10.1038/nsmb.3248
109. Johnston S, Martin M, Di Leo A, et al. MONARCH 3 final PFS: a randomized study of abemaciclib as initial therapy for advanced breast cancer. npj Breast Cancer. 2019;5(1):1-8. doi:10.1038/s41523-018-0097-z
110. Hortobagyi GN, Stemmer SM, Burris HA, et al. Ribociclib as First-Line Therapy for HR-Positive, Advanced Breast Cancer. N Engl J Med. 2016;375(18):1738-1748. doi:10.1056/nejmoa1609709
111. Knudsen ES, Witkiewicz AK. The Strange Case of CDK4/6 Inhibitors: Mechanisms, Resistance, and Combination Strategies. Trends in Cancer. 2017;3(1):39-55. doi:10.1016/j.trecan.2016.11.006
112. Béguelin W, Popovic R, Teater M, et al. EZH2 Is Required for Germinal Center Formation and Somatic EZH2 Mutations Promote Lymphoid Transformation. Cancer Cell. 2013;23(5):677-692. doi:10.1016/j.ccr.2013.04.011
113. Zhao Y, Hu Z, Li J, Hu T. EZH2 exacerbates breast cancer by methylating and activating STAT3 directly. J Cancer. 2021;12(17):5220-5230. doi:10.7150/jca.50675
114. McCabe MT, Graves AP, Ganji G, et al. Mutation of A677 in histone methyltransferase EZH2 in human B-cell lymphoma promotes hypertrimethylation of histone H3 on lysine 27 (H3K27). Proc Natl Acad Sci U S A. 2012;109(8):2989-2994. doi:10.1073/pnas.1116418109
115. Li H, Cai Q, Wu H, et al. SUZ12 promotes human epithelial ovarian cancer by suppressing apoptosis via silencing HRK. Mol Cancer Res. 2012;23(1):1-7. doi:10.1158/1541-7786.MCR-12-0335.SUZ12
116. Wu Y, Hu H, Zhang W, et al. SUZ12 is a novel putative oncogene promoting tumorigenesis in head and neck squamous cell carcinoma. J Cell Mol Med. 2018;22(7):3582-3594. doi:10.1111/jcmm.13638
117. Liu YL, Gao X, Jiang Y, et al. Expression and clinicopathological significance of EED, SUZ12 and EZH2 mRNA in colorectal cancer. J Cancer Res Clin Oncol. 2015;141(4):661-669. doi:10.1007/s00432-014-1854-5
118. Wang F, Gao Y, Lv Y, et al. Polycomb-like 2 regulates PRC2 components to affect proliferation in glioma cells. J Neurooncol. 2020;148(2):259-271. doi:10.1007/s11060-020-03538-0
119. Wu TT, Cai J, Tian YH, et al. MTF2 induces epithelial-mesenchymal transition and progression of hepatocellular carcinoma by transcriptionally activating snail. Onco Targets Ther. 2019;12:11207-11220. doi:10.2147/OTT.S226119
120. Ntziachristos P, Tsirigos A, Vlierberghe P Van, et al. Genetic inactivation of the polycomb repressive complex 2 in T cell acute lymphoblastic leukemia. Nat Med. 2012;18(2):296-301. doi:10.1038/nm.2651
121. Mieczkowska IK, Pantelaiou-Prokaki G, Prokakis E, et al. Decreased PRC2 activity supports the survival of basal-like breast cancer cells to cytotoxic treatments. Cell Death Dis. 2021;12(12).

doi:10.1038/s41419-021-04407-y
122. Michael A, Megha C, Tong AHY, Katherine C, Moffat J. Pooled Lentiviral CRISPR-Cas9 Screens for Functional Genomics in Mammalian Cells Michael. A Man Without Words. 2019;1869:158-166. doi:10.1525/9780520959316-018

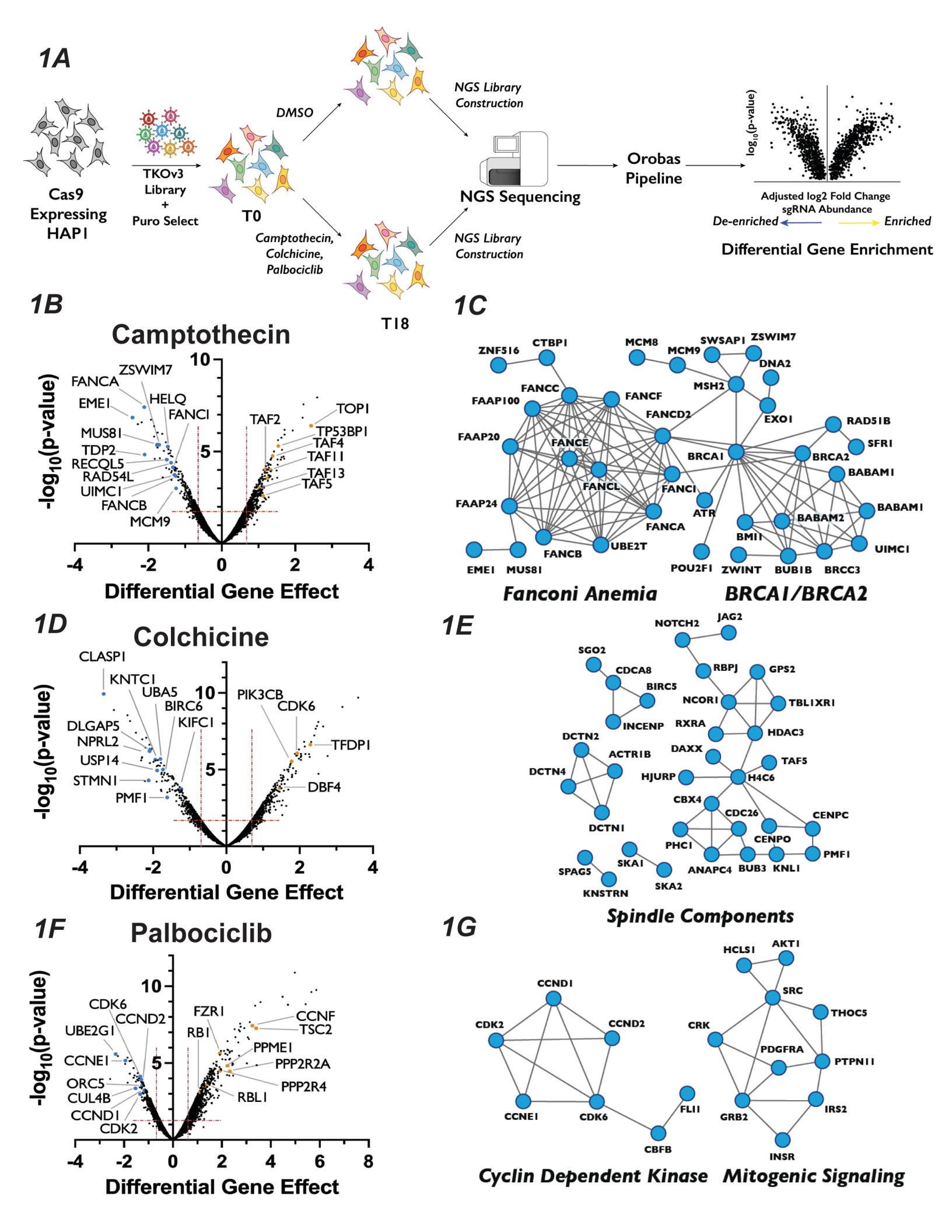
1A
Cas9 Expressing HAP1
TKOv3 Library + Puro Select
T0
DMSO
Camptothecin, Colchicine, Palbociclib
T18
NGS Library Construction
NGS Sequencing
Orobas Pipeline
Adjusted log2 Fold Change sgRNA Abundance
De-enriched
Enriched
Differential Gene Enrichment
1B
Camptothecin
-log10(p-value)
Differential Gene Effect
ZSWIM7
FANCA
EME1
HELQ
FANCI
MUS81
TDP2
RECQL5
RAD54L
UIMC1
FANCB
MCM9
TAF2
TOP1
TP53BP1
TAF4
TAF11
TAF13
TAF5
1C
ZNF516
CTBP1
MCM8
MCM9
SWSAP1
ZSWIM7
DNA2
MSH2
FANCC
FAAP100
FANCF
FANCD2
EXO1
RAD51B
SFR1
FAAP20
FANCE
BRCA1
BRCA2
BABAM1
FANCL
FANCI
FAAP24
ATR
BABAM1
BABAM2
FANCA
BMI1
UIMC1
FANCB
UBE2T
EME1
MUS81
POU2F1
ZWINT
BUB1B
BRCC3
Fanconi Anemia
BRCA1/BRCA2
1D
Colchicine
CLASP1
KNTC1
UBA5
BIRC6
KIFC1
DLGAP5
NPRL2
USP14
STMN1
PMF1
PIK3CB
CDK6
TFDP1
DBF4
1E
NOTCH2
JAG2
SGO2
CDCA8
RBPJ
GPS2
BIRC5
NCOR1
TBL1XR1
INCENP
RXRA
HDAC3
DCTN2
DAXX
ACTR1B
TAF5
DCTN4
HJURP
H4C6
CBX4
CDC26
CENPC
DCTN1
PHC1
CENPO
PMF1
SKA1
SPAG5
ANAPC4
BUB3
KNL1
KNSTRN
SKA2
Spindle Components
1F
Palbociclib
CDK6
CCND2
UBE2G1
CCNE1
ORC5
CUL4B
CCND1
CDK2
FZR1
RB1
CCNF
TSC2
PPME1
PPP2R2A
PPP2R4
RBL1
1G
HCLS1
AKT1
CCND1
SRC
THOC5
CDK2
CCND2
CRK
PDGFRA
PTPN11
CCNE1
CDK6
FLI1
GRB2
IRS2
CBFB
INSR
Cyclin Dependent Kinase
Mitogenic Signaling

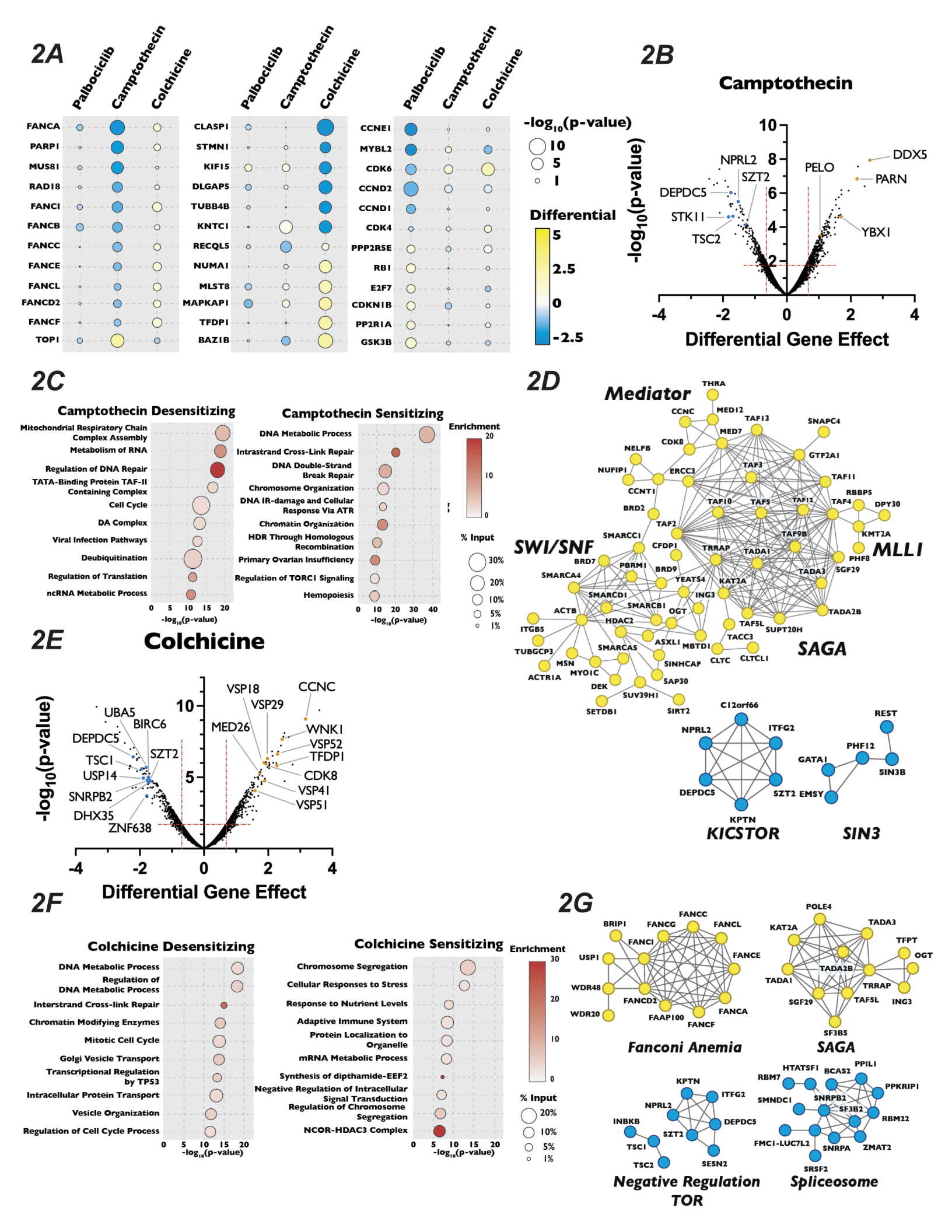
2A
Palbociclib
Camptothecin
Colchicine
FANCA
PARP1
MUS81
RAD18
FANCI
FANCB
FANCC
FANCE
FANCL
FANCD2
FANCF
TOP1
CLASP1
STMN1
KIF15
DLGAP5
TUBB4B
KNTC1
RECQL5
NUMA1
MLST8
MAPKAP1
TFDP1
BAZ1B
CCNE1
MYBL2
CDK6
CCND2
CCND1
CDK4
PPP2R5E
RB1
E2F7
CDKN1B
PP2R1A
GSK3B
-log10(p-value)
10
5
1
Differential
5
2.5
0
-2.5
2B
Camptothecin
-log10(p-value)
Differential Gene Effect
DDX5
PARN
PELO
NPRL2
SZT2
DEPDC5
STK11
TSC2
YBX1
2C
Camptothecin Desensitizing
Mitochondrial Respiratory Chain Complex Assembly
Metabolism of RNA
Regulation of DNA Repair
TATA-Binding Protein TAF-II Containing Complex
Cell Cycle
DA Complex
Viral Infection Pathways
Deubiquitination
Regulation of Translation
ncRNA Metabolic Process
-log10(p-value)
Camptothecin Sensitizing
DNA Metabolic Process
Intrastrand Cross-Link Repair
DNA Double-Strand Break Repair
Chromosome Organization
DNA IR-damage and Cellular Response Via ATR
Chromatin Organization
HDR Through Homologous Recombination
Primary Ovarian Insufficiency
Regulation of TORC1 Signaling
Hemopoiesis
-log10(p-value)
Enrichment
% Input
30%
20%
10%
5%
1%
2D
Mediator
SWI/SNF
MLL1
SAGA
KICSTOR
SIN3
2E
Colchicine
-log10(p-value)
Differential Gene Effect
VSP18
VSP29
CCNC
UBA5
BIRC6
MED26
WNK1
VSP52
TFDP1
DEPDC5
SZT2
TSC1
USP14
CDK8
SNRPB2
VSP41
VSP51
DHX35
ZNF638
2F
Colchicine Desensitizing
DNA Metabolic Process
Regulation of DNA Metabolic Process
Interstrand Cross-link Repair
Chromatin Modifying Enzymes
Mitotic Cell Cycle
Golgi Vesicle Transport
Transcriptional Regulation by TP53
Intracellular Protein Transport
Vesicle Organization
Regulation of Cell Cycle Process
-log10(p-value)
Colchicine Sensitizing
Chromosome Segregation
Cellular Responses to Stress
Response to Nutrient Levels
Adaptive Immune System
Protein Localization to Organelle
mRNA Metabolic Process
Synthesis of dipthamide-EEF2
Negative Regulation of Intracellular Signal Transduction
Regulation of Chromosome Segregation
NCOR-HDAC3 Complex
-log10(p-value)
Enrichment
% Input
20%
10%
5%
1%
2G
Fanconi Anemia
SAGA
Negative Regulation TOR
Spliceosome

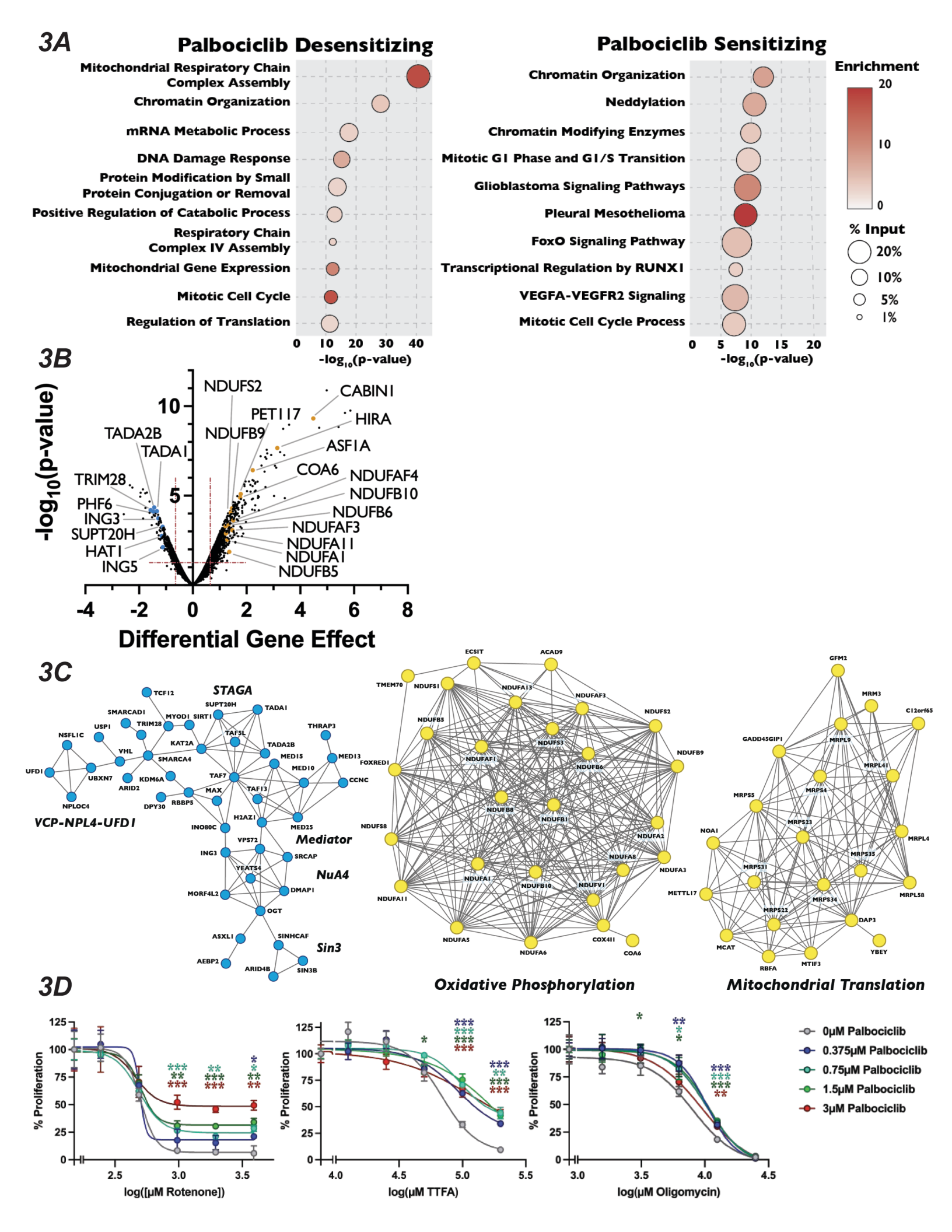
3A
Palbociclib Desensitizing
Mitochondrial Respiratory Chain Complex Assembly
Chromatin Organization
mRNA Metabolic Process
DNA Damage Response
Protein Modification by Small Protein Conjugation or Removal
Positive Regulation of Catabolic Process
Respiratory Chain Complex IV Assembly
Mitochondrial Gene Expression
Mitotic Cell Cycle
Regulation of Translation
0 10 20 30 40
-log10(p-value)
Palbociclib Sensitizing
Chromatin Organization
Neddylation
Chromatin Modifying Enzymes
Mitotic G1 Phase and G1/S Transition
Glioblastoma Signaling Pathways
Pleural Mesothelioma
FoxO Signaling Pathway
Transcriptional Regulation by RUNX1
VEGFA-VEGFR2 Signaling
Mitotic Cell Cycle Process
0 5 10 15 20
-log10(p-value)
Enrichment
20
10
0
% Input
20%
10%
5%
1%
3B
-log10(p-value)
Differential Gene Effect
NDUFS2
CABIN1
PET117
HIRA
TADA2B
NDUFB9
TADA1
ASF1A
COA6
TRIM28
NDUFAF4
NDUFB10
PHF6
ING3
NDUFB6
SUPT20H
NDUFAF3
HAT1
NDUFA11
ING5
NDUFA1
NDUFB5
3C
STAGA
TCF12
SUPT20H
TADA1
SMARCAD1
MYOD1
SIRT1
TRIM28
USP1
NSFL1C
TAF5L
THRAP3
KAT2A
TADA2B
VHL
SMARCA4
MED15
MED13
UFD1
UBXN7
MED10
KDM6A
CCNC
ARID2
TAF7
NPLOC4
MAX
TAF13
DPY30
RBBP5
VCP-NPL4-UFD1
H2AZ1
MED25
INO80C
Mediator
VPS72
ING3
SRCAP
YEATS4
NuA4
MORF4L2
DMAP1
OGT
ASXL1
SINHCAF
Sin3
AEBP2
ARID4B
SIN3B
ECSIT
ACAD9
TMEM70
NDUFS1
NDUFA13
NDUFAF3
NDUFS2
NDUFB5
NDUFS3
NDUFAF1
NDUFB9
FOXRED1
NDUFB6
NDUFB8
NDUFB1
NDUFS8
NDUFA2
NDUFA8
NDUFA3
NDUFA1
NDUFB10
NDUFV1
NDUFA11
NDUFA5
NDUFA6
COX4I1
COA6
Oxidative Phosphorylation
GFM2
MRM3
C12orf65
GADD45GIP1
MRPL9
MRPL41
MRPS5
MRPS54
MRPS23
NOA1
MRPL4
MRPS35
MRPS31
METTL17
MRPS34
MRPL58
MRPS22
DAP3
MCAT
YBEY
RBFA
MTIF3
Mitochondrial Translation
3D
% Proliferation
log([μM Rotenone])
log(μM TTFA)
log(μM Oligomycin)
0μM Palbociclib
0.375μM Palbociclib
0.75μM Palbociclib
1.5μM Palbociclib
3μM Palbociclib

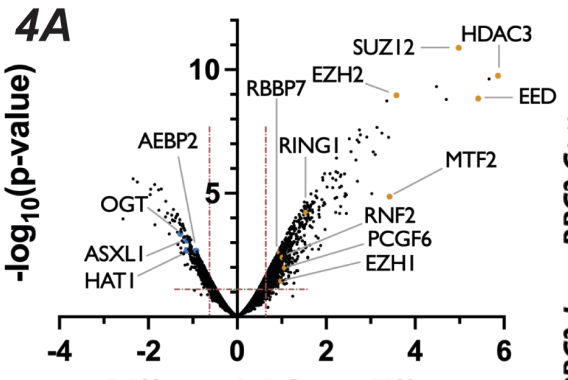
4A
-log10(p-value)
Differential Gene Effect
SUZ12
HDAC3
EZH2
RBBP7
EED
AEBP2
RING1
MTF2
OGT
RNF2
PCGF6
ASXL1
EZH1
HAT1

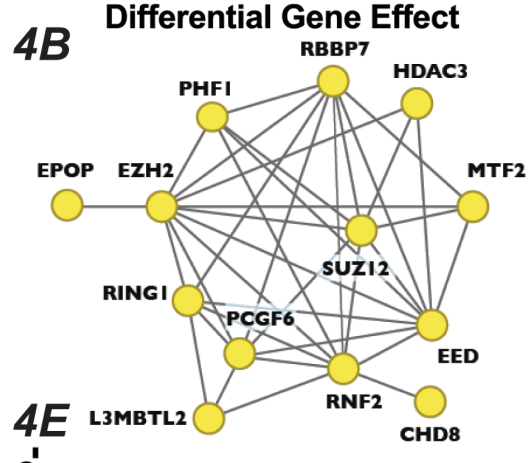
4B
RBBP7
PHF1
HDAC3
EPOP
EZH2
MTF2
SUZ12
RING1
PCGF6
EED
RNF2
L3MBTL2
CHD8

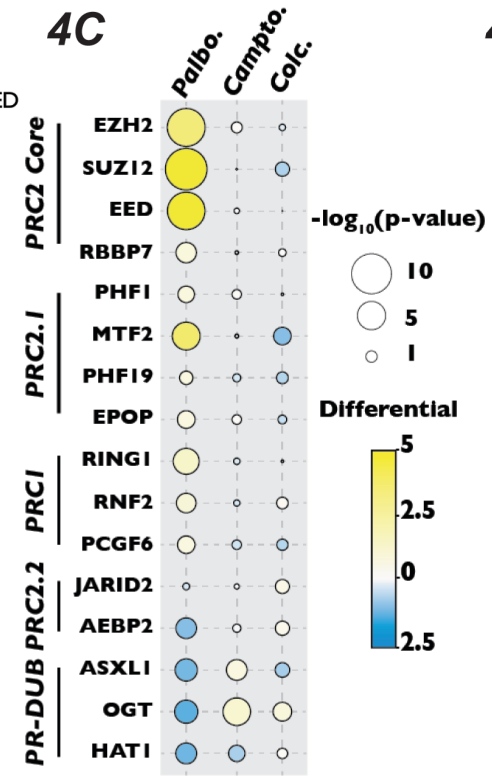
4C
Palbo.
Campto.
Colc.
PRC2 Core
EZH2
SUZ12
EED
RBBP7
PRC2.1
PHF1
MTF2
PHF19
EPOP
PRC1
RING1
RNF2
PCGF6
PRC2.2
JARID2
AEBP2
PR-DUB
ASXL1
OGT
HAT1
-log10(p-value)
10
5
1
Differential
5
2.5
0
-2.5

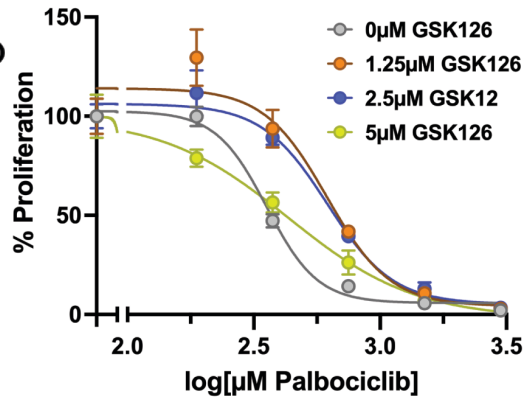
4D
0μM GSK126
1.25μM GSK126
2.5μM GSK12
5μM GSK126
% Proliferation
log[μM Palbociclib]

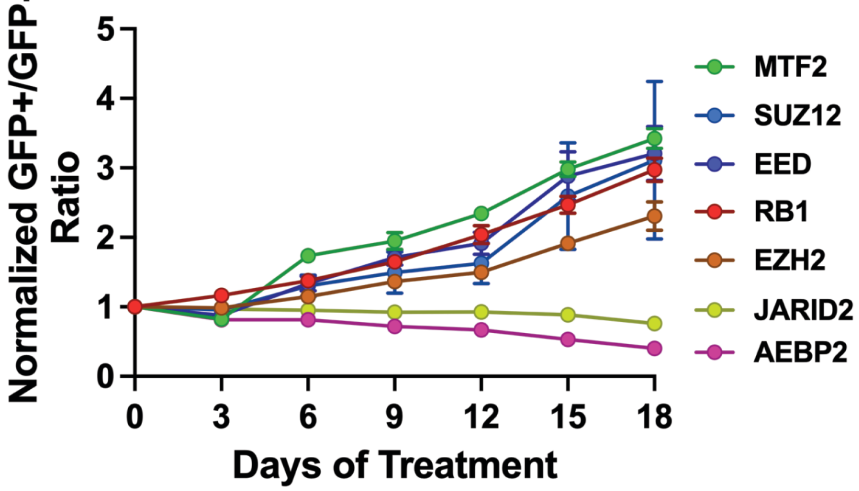
4E
Normalized GFP+/GFP- Ratio
Days of Treatment
MTF2
SUZ12
EED
RB1
EZH2
JARID2
AEBP2

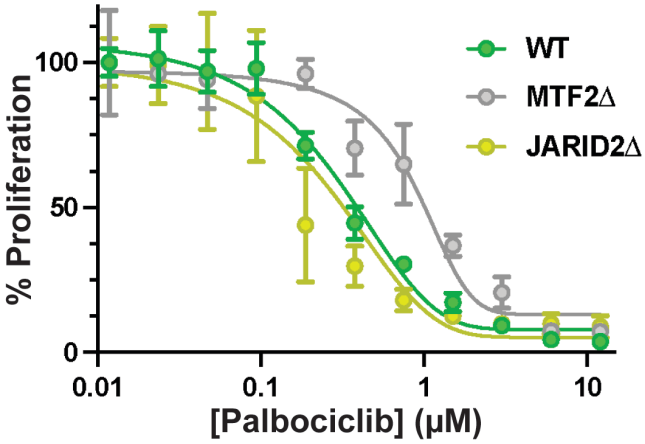
4F
WT
MTF2Δ
JARID2Δ
% Proliferation
[Palbociclib] (μM)

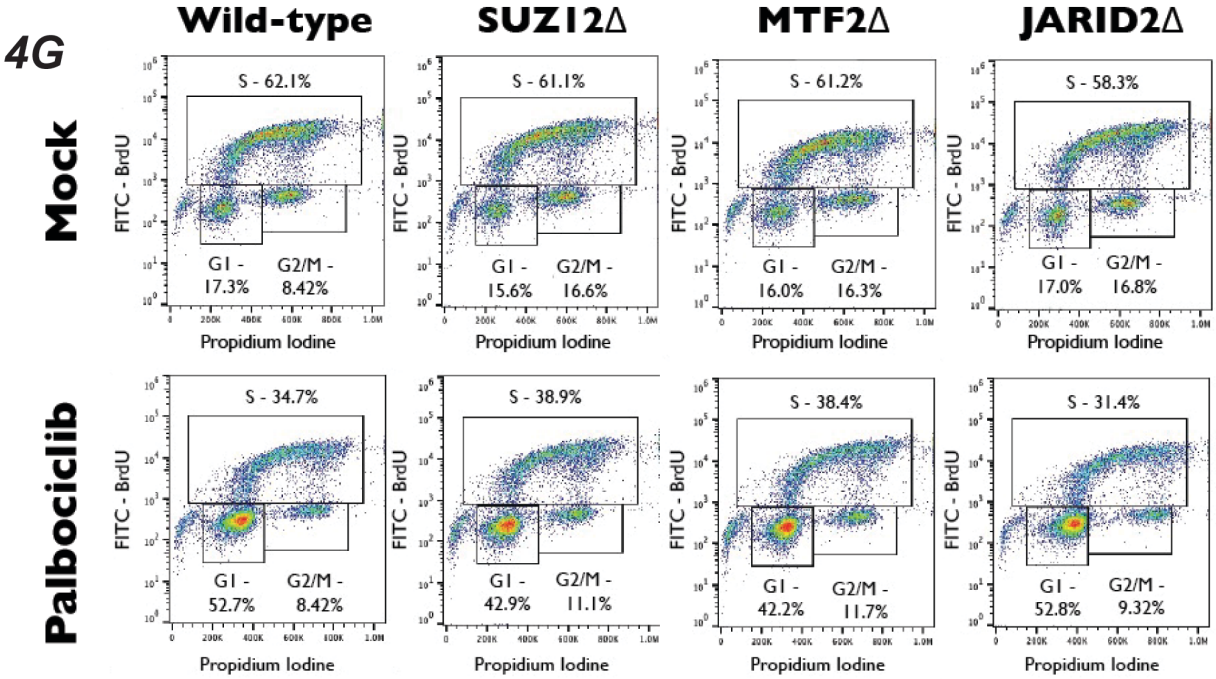
4G
Wild-type
SUZ12Δ
MTF2Δ
JARID2Δ
Mock
Palbociclib
FITC - BrdU
Propidium Iodine
S - 62.1%
G1 - 17.3%
G2/M - 8.42%
S - 61.1%
G1 - 15.6%
G2/M - 16.6%
S - 61.2%
G1 - 16.0%
G2/M - 16.3%
S - 58.3%
G1 - 17.0%
G2/M - 16.8%
S - 34.7%
G1 - 52.7%
G2/M - 8.42%
S - 38.9%
G1 - 42.9%
G2/M - 11.1%
S - 38.4%
G1 - 42.2%
G2/M - 11.7%
S - 31.4%
G1 - 52.8%
G2/M - 9.32%

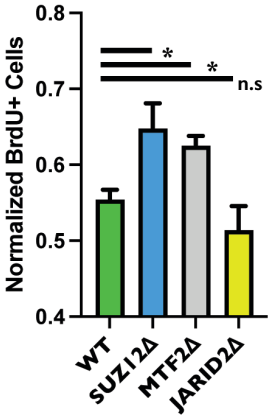
Normalized BrdU+ Cells
*
*
n.s
WT
SUZ12Δ
MTF2Δ
JARID2Δ

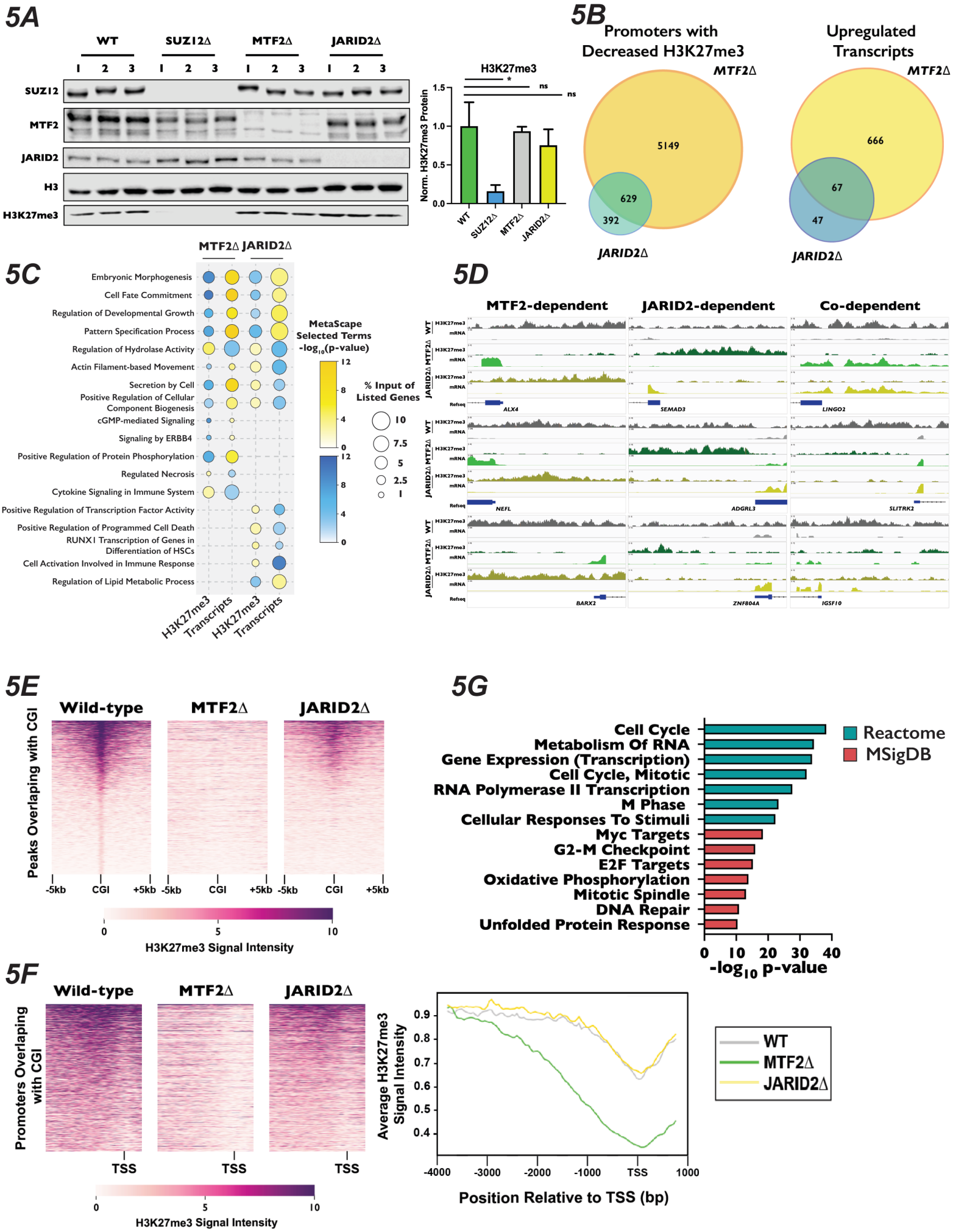
5A
WT
SUZ12Δ
MTF2Δ
JARID2Δ
1 2 3 1 2 3 1 2 3 1 2 3
SUZ12
MTF2
JARID2
H3
H3K27me3
H3K27me3
Norm. H3K27me3 Protein
1.5
1.0
0.5
0.0
*
ns
ns
WT
SUZ12Δ
MTF2Δ
JARID2Δ
5B
Promoters with Decreased H3K27me3
MTF2Δ
5149
629
392
JARID2Δ
Upregulated Transcripts
MTF2Δ
666
67
47
JARID2Δ
5C
MTF2Δ JARID2Δ
Embryonic Morphogenesis
Cell Fate Commitment
Regulation of Developmental Growth
Pattern Specification Process
Regulation of Hydrolase Activity
Actin Filament-based Movement
Secretion by Cell
Positive Regulation of Cellular Component Biogenesis
cGMP-mediated Signaling
Signaling by ERBB4
Positive Regulation of Protein Phosphorylation
Regulated Necrosis
Cytokine Signaling in Immune System
Positive Regulation of Transcription Factor Activity
Positive Regulation of Programmed Cell Death
RUNX1 Transcription of Genes in Differentiation of HSCs
Cell Activation Involved in Immune Response
Regulation of Lipid Metabolic Process
H3K27me3
Transcripts
H3K27me3
Transcripts
MetaScape Selected Terms -log10(p-value)
12
8
4
0
12
8
4
0
% Input of Listed Genes
10
7.5
5
2.5
1
5D
MTF2-dependent
JARID2-dependent
Co-dependent
WT
MTF2Δ
JARID2Δ
H3K27me3
mRNA
Refseq
ALX4
SEMAD3
LINGO2
NEFL
ADGRL3
SLITRK2
BARX2
ZNF804A
IGSF10
5E
Wild-type
MTF2Δ
JARID2Δ
Peaks Overlaping with CGI
-5kb
CGI
+5kb
0
5
10
H3K27me3 Signal Intensity
5G
Cell Cycle
Metabolism Of RNA
Gene Expression (Transcription)
Cell Cycle, Mitotic
RNA Polymerase II Transcription
M Phase
Cellular Responses To Stimuli
Myc Targets
G2-M Checkpoint
E2F Targets
Oxidative Phosphorylation
Mitotic Spindle
DNA Repair
Unfolded Protein Response
Reactome
MSigDB
0 10 20 30 40
-log10 p-value
5F
Wild-type
MTF2Δ
JARID2Δ
Promoters Overlaping with CGI
TSS
0
5
10
H3K27me3 Signal Intensity
Average H3K27me3 Signal Intensity
0.9
0.8
0.7
0.6
0.5
0.4
-4000
-3000
-2000
-1000
TSS
1000
Position Relative to TSS (bp)
WT
MTF2Δ
JARID2Δ

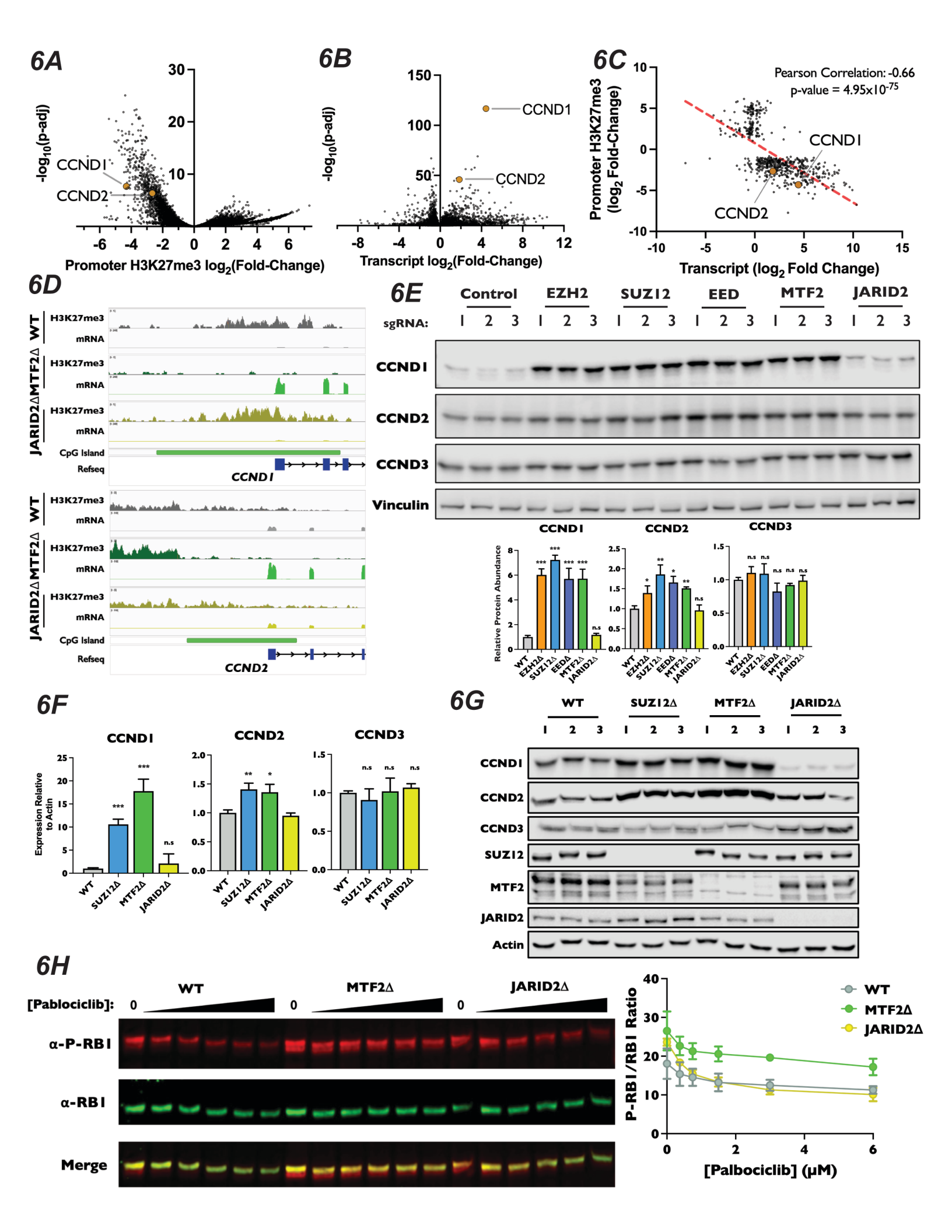
6A
-log10(p-adj)
CCND1
CCND2
Promoter H3K27me3 log2(Fold-Change)
6B
-log10(p-adj)
CCND1
CCND2
Transcript log2(Fold-Change)
6C
Pearson Correlation: -0.66
p-value = 4.95x10-75
Promoter H3K27me3 (log2 Fold-Change)
CCND1
CCND2
Transcript (log2 Fold Change)
6D
WT
MTF2Δ
JARID2Δ
H3K27me3
mRNA
CpG Island
Refseq
CCND1
CCND2
6E
Control
EZH2
SUZ12
EED
MTF2
JARID2
sgRNA:
CCND1
CCND2
CCND3
Vinculin
Relative Protein Abundance
WT
EZH2Δ
SUZ12Δ
EEDΔ
MTF2Δ
JARID2Δ
6F
CCND1
CCND2
CCND3
Expression Relative to Actin
WT
SUZ12Δ
MTF2Δ
JARID2Δ
6G
WT
SUZ12Δ
MTF2Δ
JARID2Δ
CCND1
CCND2
CCND3
SUZ12
MTF2
JARID2
Actin
6H
[Pablociclib]:
WT
MTF2Δ
JARID2Δ
α-P-RB1
α-RB1
Merge
P-RB1/RB1 Ratio
[Palbociclib] (μM)

S1A

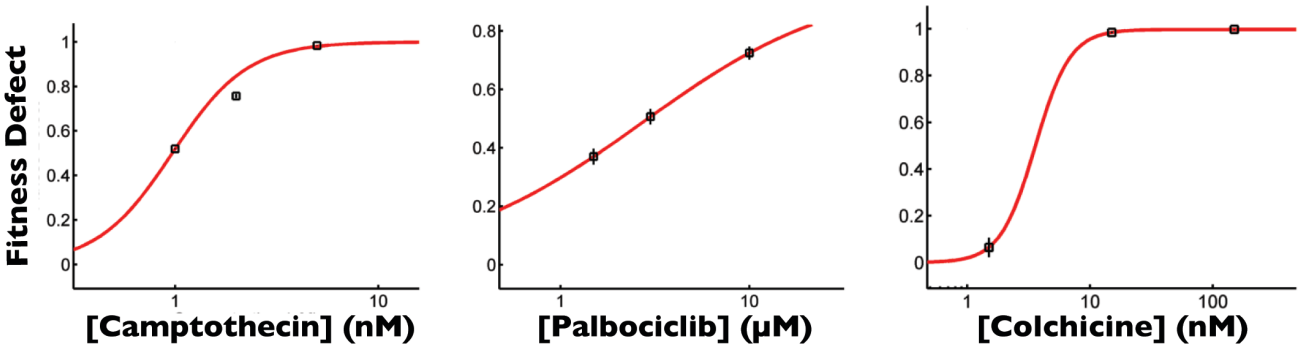
Fitness Defect
[Camptothecin] (nM)
[Palbociclib] (μM)
[Colchicine] (nM)

S1B

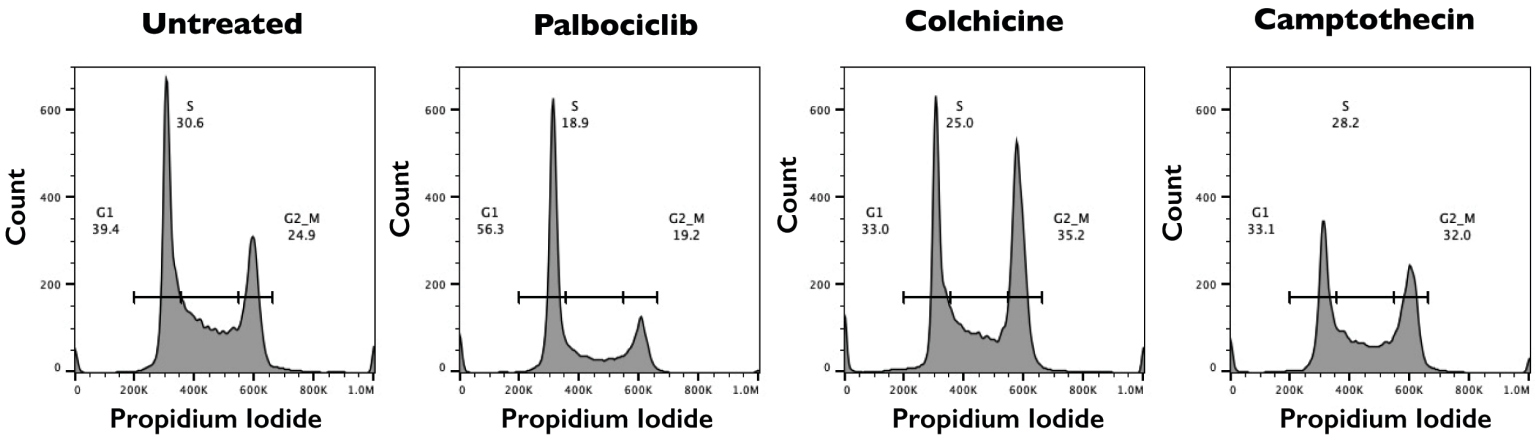
Untreated
Palbociclib
Colchicine
Camptothecin
Count
Propidium Iodide
S 30.6
G1 39.4
G2_M 24.9
S 18.9
G1 56.3
G2_M 19.2
S 25.0
G1 33.0
G2_M 35.2
S 28.2
G1 33.1
G2_M 32.0

S1C

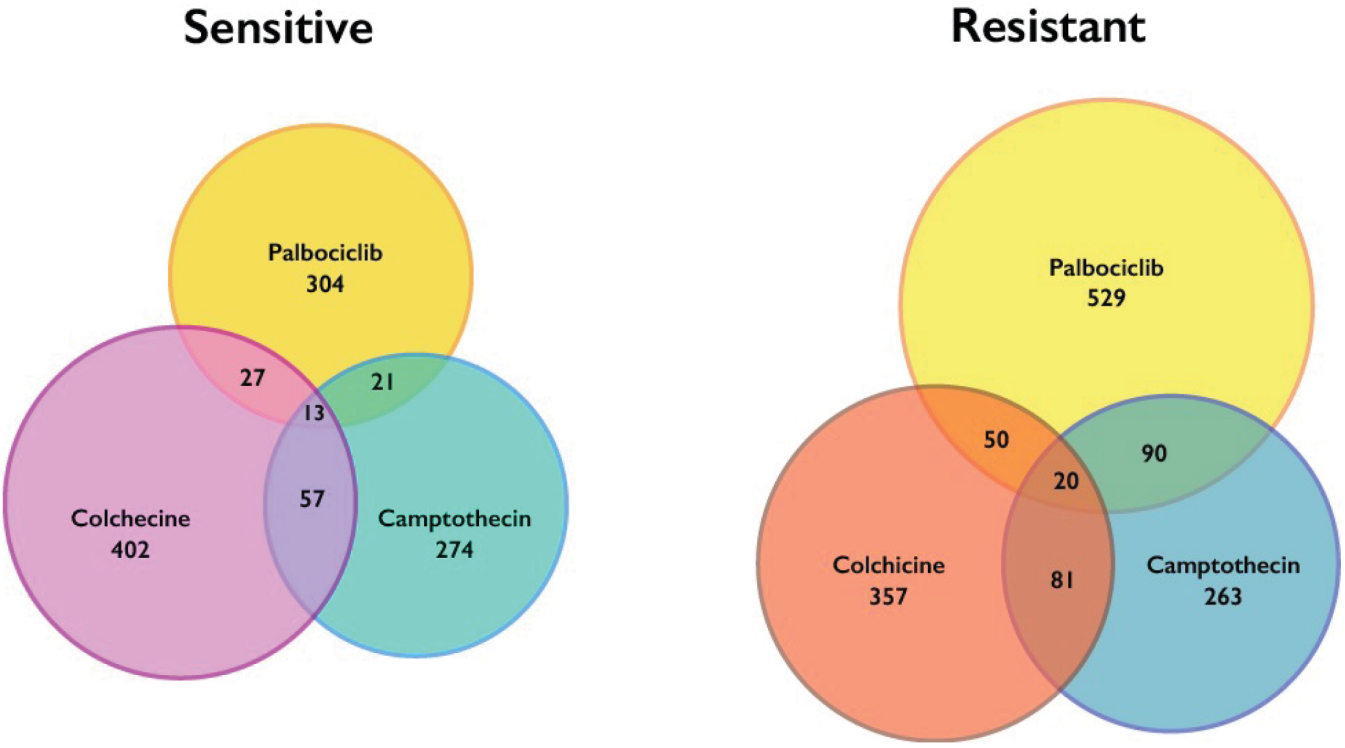
Sensitive
Palbociclib 304
Colchecine 402
Camptothecin 274
27
21
13
57
Resistant
Palbociclib 529
Colchicine 357
Camptothecin 263
50
90
20
81

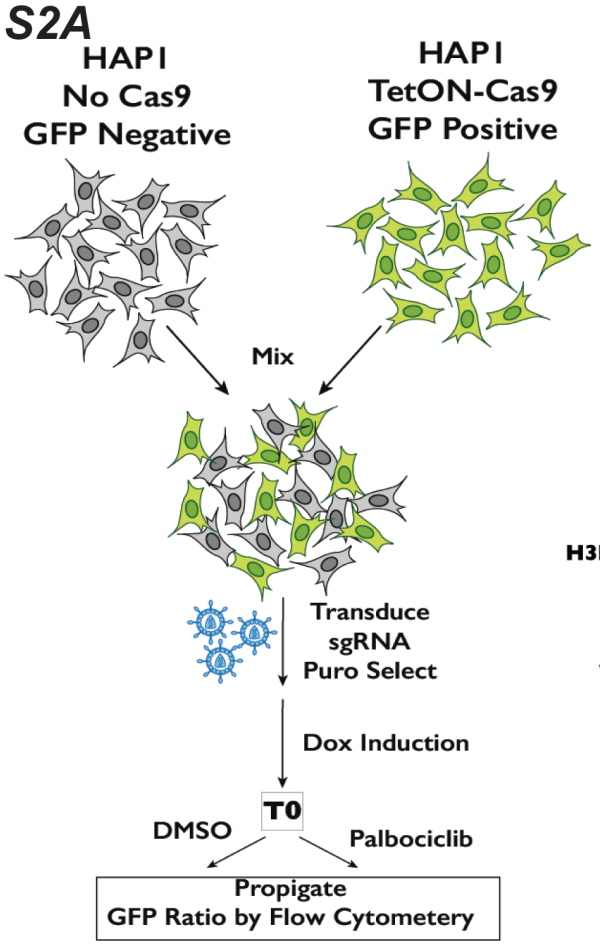
S2A
HAP1
No Cas9
GFP Negative
HAP1
TetON-Cas9
GFP Positive
Mix
Transduce
sgRNA
Puro Select
Dox Induction
T0
DMSO
Palbociclib
Propigate
GFP Ratio by Flow Cytometery

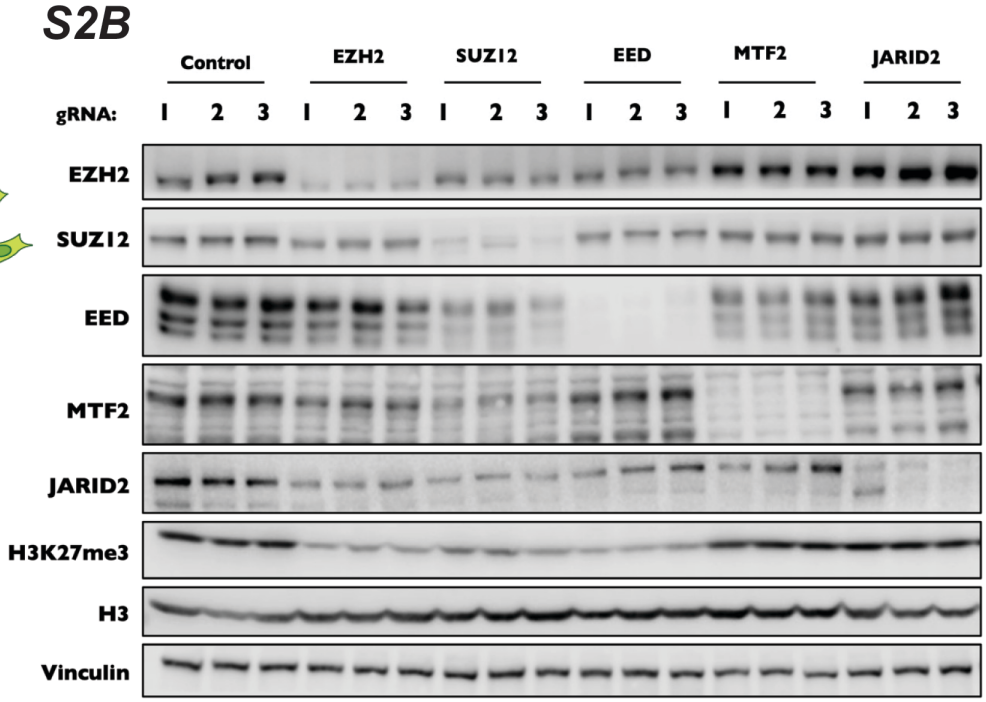
S2B
Control
EZH2
SUZ12
EED
MTF2
JARID2
gRNA:
1 2 3 1 2 3 1 2 3 1 2 3 1 2 3 1 2 3
EZH2
SUZ12
EED
MTF2
JARID2
H3K27me3
H3
Vinculin

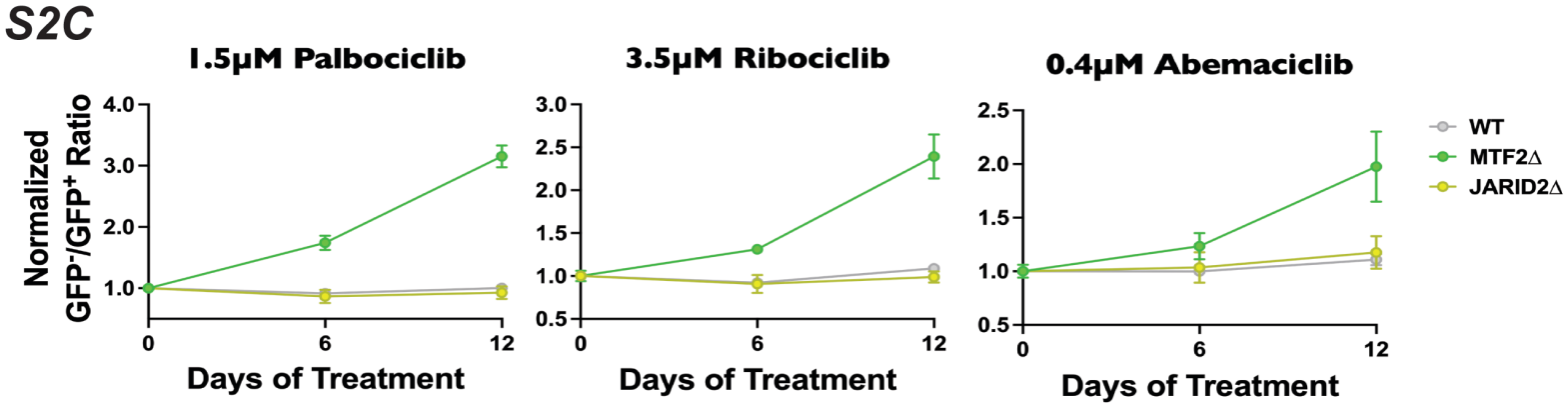
S2C
1.5μM Palbociclib
3.5μM Ribociclib
0.4μM Abemaciclib
Normalized GFP⁻/GFP⁺ Ratio
Days of Treatment
WT
MTF2Δ
JARID2Δ

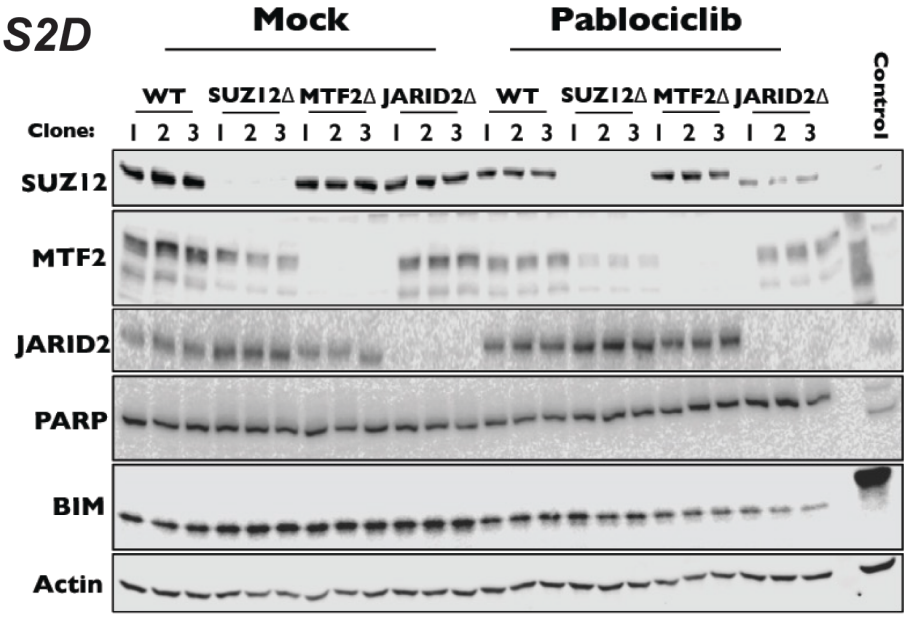
S2D
Mock
Pablociclib
WT
SUZ12Δ
MTF2Δ
JARID2Δ
Control
Clone:
1 2 3
SUZ12
MTF2
JARID2
PARP
BIM
Actin

S3A

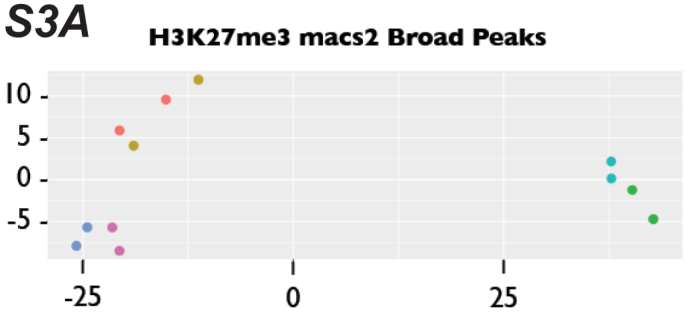

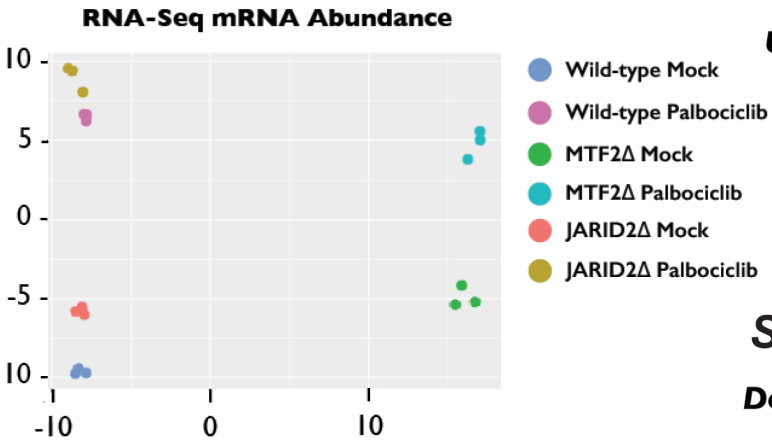

S3B

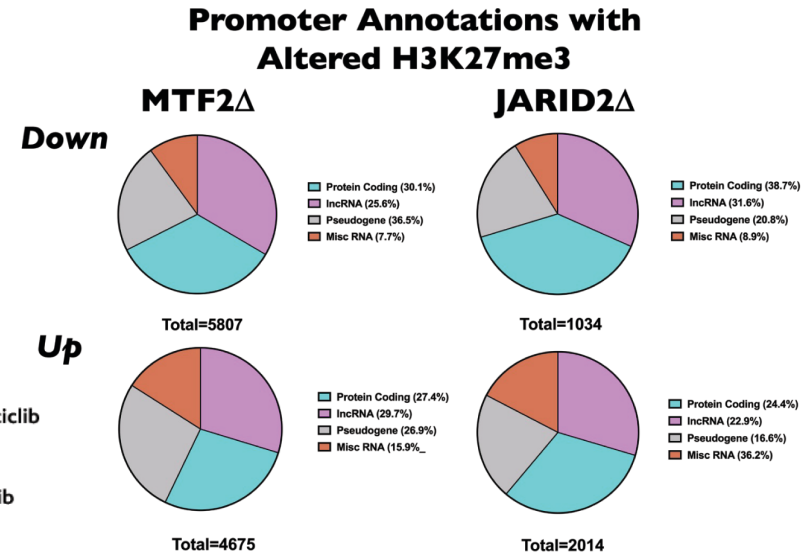

S3C

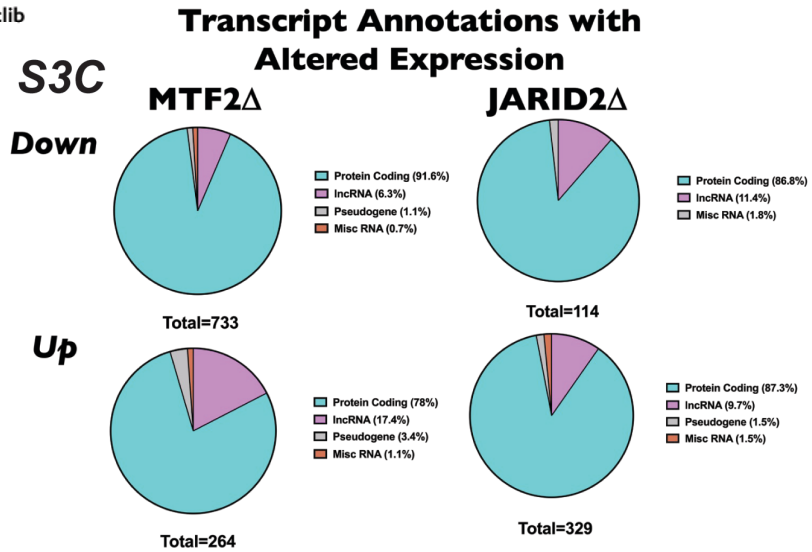

S3D

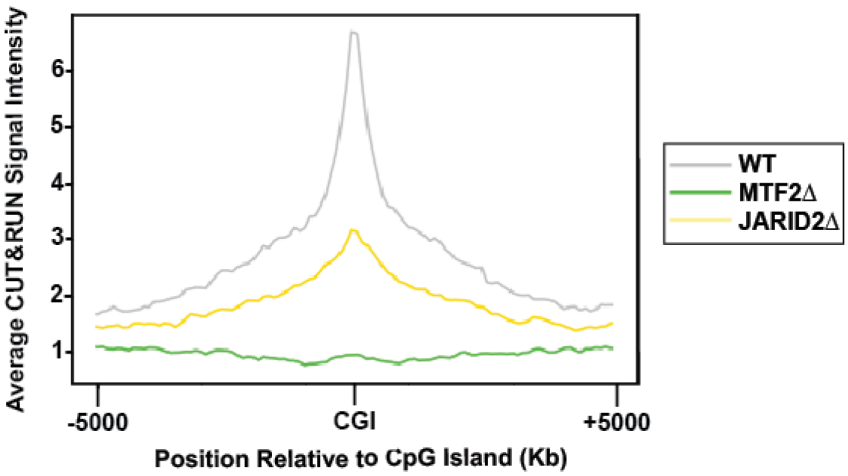

S3E

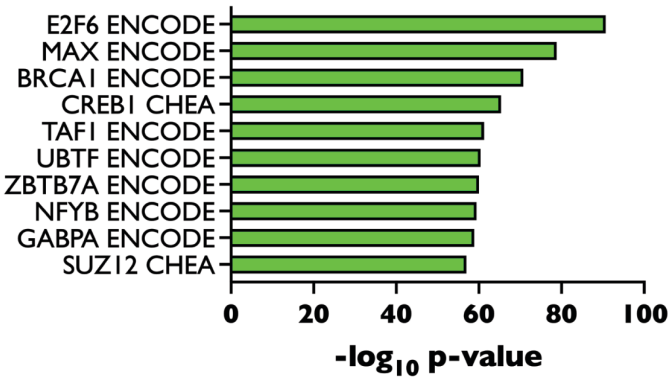

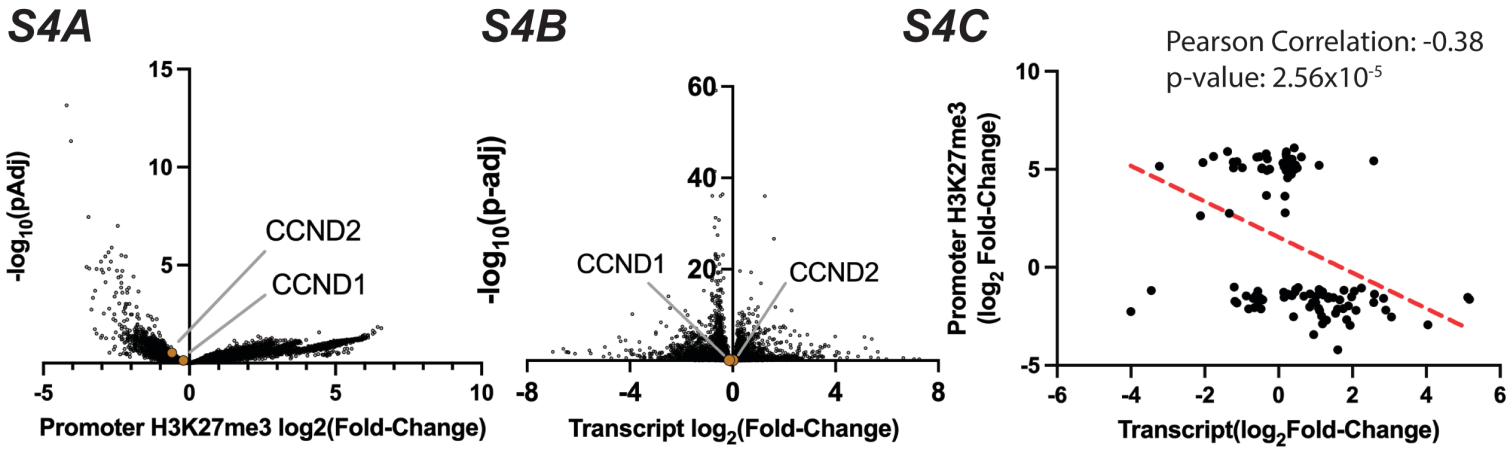
S4A
S4B
S4C
-log10(pAdj)
CCND2
CCND1
Promoter H3K27me3 log2(Fold-Change)
-log10(p-adj)
CCND1
CCND2
Transcript log2(Fold-Change)
Pearson Correlation: -0.38
p-value: 2.56x10-5
Promoter H3K27me3 (log2 Fold-Change)
Transcript(log2Fold-Change)

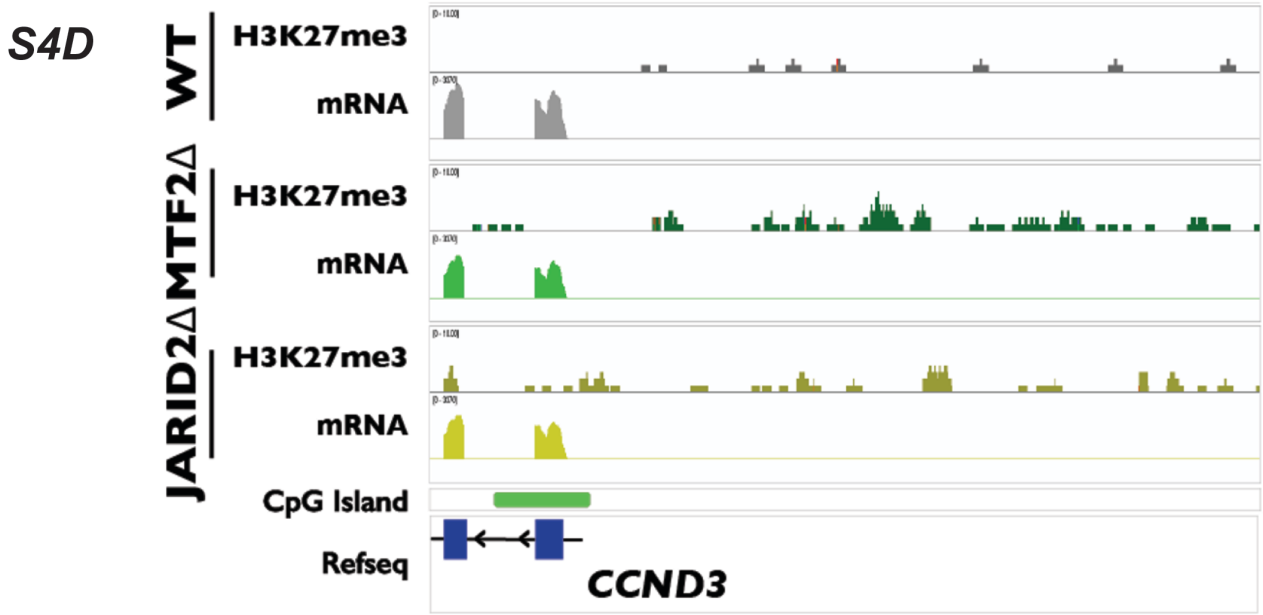
S4D
WT
H3K27me3
mRNA
MTF2Δ
H3K27me3
mRNA
JARID2Δ
H3K27me3
mRNA
CpG Island
Refseq
CCND3

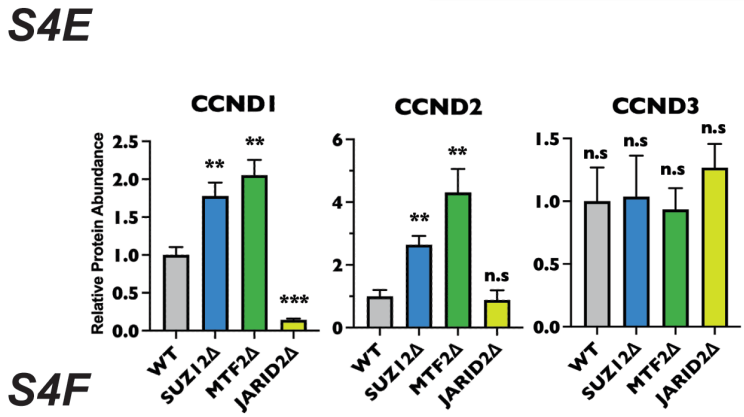
S4E
CCND1
CCND2
CCND3
Relative Protein Abundance
WT
SUZ12Δ
MTF2Δ
JARID2Δ

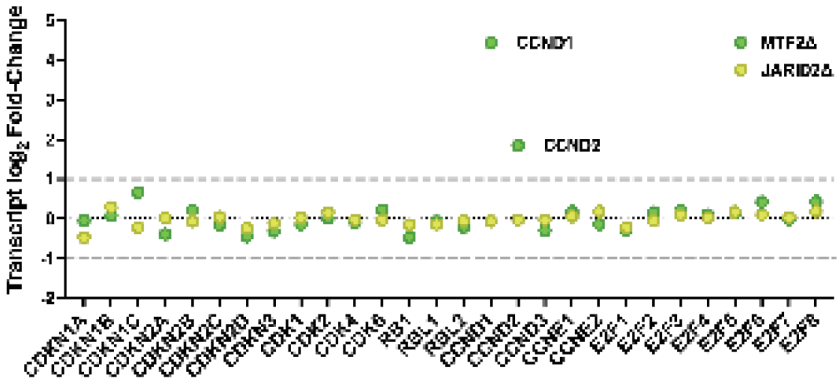
S4F
Transcript log2 Fold-Change
CCND1
CCND2
MTF2Δ
JARID2Δ

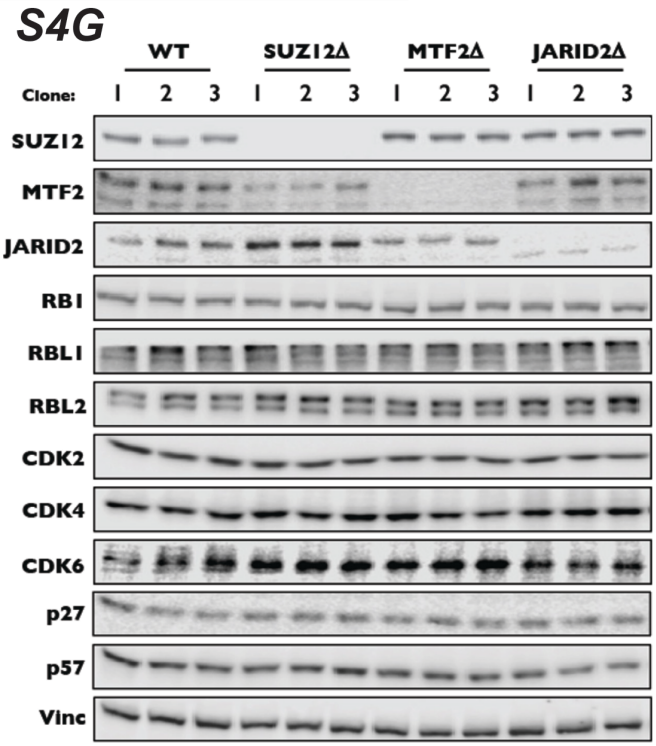
S4G
WT
SUZ12Δ
MTF2Δ
JARID2Δ
Clone:
SUZ12
MTF2
JARID2
RB1
RBL1
RBL2
CDK2
CDK4
CDK6
p27
p57
Vinc